Skarn Evolution and Hydrothermal Fluid Characteristics in the Nickel Plate Deposit, Hedley District, British Columbia, Canada

509 - 334-0926

Art D. Ettlinger and Lawrence D. Meinert
Department of Geology, Washington State University
Pullman, WA 99165

and

Gerry E. Ray
British Columbia Geological Survey
Victoria, BC V8V 1X4

Skarn Evolution and Hydrothermal Fluid Characteristics in the Nickel Plate Deposit, Hedley District, British Columbia, Canada

Art D. Ettlinger and Lawrence D. Meinert
Department of Geology, Washington State University
Pullman, WA 99165
and
Gerry E. Ray
British Columbia Geological Survey
Victoria, BC V8V 1X4

Abstract

The Nickel Plate ore body in the Hedley district Is the largest gold skarn deposit in Canada. During the period 1904-1955 it produced almost 49 million grams of gold representing approximately half of the gold produced from all skarns in British Columbia. The deposit it hosted by thinly bedded calcareous and tuffaceous siltstones and limestones of the Upper Triassic Nicola Group, an accreted oceanic arc assemblage. These rocks are intruded by numerous sills, dikes and small stocks of sub-alkalic, calc-alkaline quartz diorite and diorite. Skarn alteration and related gold mineralization overprints sedimentary and igneous rock and is zoned about the intrusive contacts.

Skarn in the Nickel Plate deposit is pyroxene-rich and is characterized by hedenbergitic pyroxene and aluminous garnet with an ore bearing assemblage of asp-po-Bi-tellurides-Au. The early stages of alteration are marked by the formation of biotite and quartz hornfels in siltstone and potassic alteration of intrusive rock. The biotite contains <0.55 mole fraction phlogopite and <2 wt % TiO_2 which are indicative of the reduced nature of this mineralization compared to porphyry-Cu systems. This early stage of alteration is continuous into formation of pyroxene skamoid which consists of intermediate pyroxene (Hd_{48-59}) in siltstone and Mg-rich pyroxene (Hd_{5-30}) and k-spar in intrusive rocks. The most volumetrically important alteration style, and the primary host to gold mineralization, consists of dark green, fine grained pyroxene (Hd_{60-94}) and lesser grandite garnet (Ad_{14-82}, ave. Ad_{35}) which overprints earlier hornfels and skarnoid, and often completely replaces both sedimentary and igneous protoliths. Ore bearing sulfides and scapolite occur with the hedenbergite skarn and consist of pyrrhotite, arsenopyrite with inclusions of Au, hedleyite and Bi, minor chalcopyrite, sphalerite and galeha. Retrograde alteration in the deposit is limited, with only minor to trace amounts of wollastonite, prehnite, epidote and chlorite replacing garnet and pyroxene.

Fluid inclusion homogenization temperatures indicate the main body of pyroxene-garnet skarn formed at an average temperature (pressure corrected) between 460-480°C with locally high temperatures of 700-800°C. Fluid salinities averaged 18.3 and 9.7 wt % NaCl equivalent for garnet and pyroxene respectively. Dissolution temperatures of halite daughters in pyroxene and quartz from skarn indicate a maximum fluid salinity of 37.9 wt % NaCl equivalent. Homogenization temperatures in scapolite associated with sulfide mineralization, indicate a lower temperature for this mineralization in the range 320-400°C.

Estimated physiochemical conditions of formation based on the composition and stability fields of major calc-silicate and sulfide minerals indicate the hedenbergite skarn, pyrrhotite and arsenopyrite were deposited under similar conditions of sulfur fugacity (log fS_2=-10 to -2) and temperature (400-650°C); while a log fO_2=-25 to -22 is estimated for the hedenbergite skarn.

Spatial trends in pyroxene and garnet composition and the distribution of fluid inclusion homogenization temperatures indicate the eastern contact of the Toronto stock and the locus of diorite dikes, such as the South dike, in the ore zone acted as critical conduits for channeling of hyrdrothermal fluids. These two separate fluid paths may have resulted in the two different compositional trends found in pyroxene and garnet from locations in the ore zone versus those more proximal to the Toronto stock.

Introduction

The Nickel Plate deposit, approximately 225 kilometers east of Vancouver in southern British Columbia, is the largest and economically most important gold skarn deposit in Canada (Fig. 1). Located in the Hedley mining district, the Nickel Plate ore body produced almost 49 million grams of gold during the period 1904-1955 (Ray et al., 1987). This represents over 95 percent of the total gold production from the Hedley district, and 51 percent of the total gold produced from all skarn deposits in British Columbia (Ettlinger and Ray, 1989).

The first detailed account of the geology of the Hedley district is by Camsell (1910). Bostock (1930, 1940a, 1940b) also mapped portions of the district, and several workers have studied the Nickel Plate deposit and surrounding areas of known mineralization in various detail (Warren and Cummings, 1936; Billingsley and Hume, 1941; Dolmage and Brown, 1945; and Lee, 1951). While these studies have resulted in a large descriptive base for the deposits of the Hedley district, they do not attempt to synthesize district geology with skarn alteration and/or gold mineralization, nor do they answer questions relating to evolution of the hydrothermal system and relationship between subsequent skarn and ore formation. Recent work by the British Columbia Geological Survey and Mascot Gold Mines Ltd. has added much to the data base of these deposits in light of what is currently understood about gold skarn deposits (Ray et al., 1986; Simpson and Ray, 1986; Ray et al., 1987; Ray and Dawson, 1987, 1988; Ettlinger and Ray, 1988, 1989). The present paper focuses on the mineralogy, petrogenesis and hydrothermal fluid characteristics of the Nickel Plate ore body. Data from over 400 electron microprobe mineral analyses, 117 fluid inclusion

analyses, and detailed logging of diamond drill core suggest that the temperature of skarn formation, alteration sequence and sulfide mineral assemblage in the Nickel Plate gold skarn system is distinct from base metal skarn deposits and that there are similarities and important differences between the Nickel Plate deposit and other Cordilleran gold skarns.

Geologic Setting

The deposit is located near the top of Nickel Plate Mountain, 3 km northeast of the town of Hedley. The region is part of the Interior Plateau of south central British Columbia which in the vicinity of Hedley, has been deeply incised by the Similkameen River and its tributaries. Over 1,300 m of relief exists between the town of Hedley at 520 m and the top of Nickel Plate Mountain. The current minesite is located on the eastern slope of the mountain at an elevation of 1 700 m.

Mining activity in the Hedley area started in 1860 with the first instance of placer mining. Mineral claims were first located on Nickel Plate Mountain in 1894 with development on the property begining in 1899. Gold production was initiated in 1904 and continued with intermittent interuptions until 1955. During its early years, Nickel Plate was one of Canada's largest gold producers (Camsell, 1910). Corona Corporation (formerly Mascot Gold Mines Ltd.) is currently mining the Nickel Plate deposit via open pit and underground operations. Mineable ore reserves as of January 1, 1989 are 5.1 million tonnes averaging 2.98 grams gold per tonne (Corona Corp. Annual Report for 1988).

The Hedley district is situated within the Intermontane belt in the southern part of the Canadian Cordillera (Fig. 1). The Intermontane Belt is a mosaic of individual fault-bounded terranes consisting primarily of Lower Paleozoic through Jurassic marine volcanic and sedimentary rocks and comagmatic intrusive rocks deposited in an island arc or marginal basin setting (Wheeler et al., 1988). These terranes were

amalgamated to form the framework of the Intermontane belt by latest Triassic time, the resulting large superterrane then accreted to the continental margin in the Jurassic.

Arc-related marine volcanic and sedimentary rocks of the Late Triassic to Early Jurassic Nicola Group host the ore deposits of the Hedley district (Rice, 1947, Ray et al., 1986). Submarine and subaerial volcanic breccia, augite and feldspar porphyry, crystal-lithic tuff, argillite, siltstone and reefoidal limestone form a belt up to 70 km wide and 190 km long in southern British Columbia where it defines the main portion of the Quesnellia terrane (Preto, 1977; Mortimer, 1986). Rocks of similar age and affinity occur futher north in Quesnellia and to the south in the U.S. (Mortimer, 1986). These Nicola Belt rocks are the host to several porphyry Cu-Mo and Cu-Ag-Au deposits and other gold skarn occurrences in addition to the deposits in the Hedley district (Preto, 1972; Barr, et al., 1976; Ettlinger and Ray, 1989).

The oldest rocks in the Hedley district belong to the highly deformed Paleozoic through Triassic Apex Mountain ophiolite complex (Fig. 1) which is separated from later Nicola Belt rocks further west by intrusions or major faults. No known gold skarn mineralization is hosted by this sequence.

Sedimentary and volcanic rocks of the Nicola Group are separated into three distinct stratigraphic sequences in the Hedley district (Ray et al., 1988). The French Mine, Hedley and Stemwinder Mountain Formations represent shallow, intermediate and deep water facies deposited along the margin of a westerly deepening, fracture controlled back-arc basin.

The easternmost French Mine Formation hosts gold skarn mineralization at the Goodhope and French mines in the Hedley district (Fig. 1). It consists of massive and bedded limestones with interlayered units of calcareous siltstone, chert pebble conglomerate and limestone breccia.

Clastic-rich rocks of the Hedley sequence lie further west and are deeper water stratigraphic equivalents to the French Mine Formation (Ray et al., 1988). This sequence is over 400 m thick and is comprised of thinly bedded calcareous and tuffaceous siltstones, limestone, argillite and minor conglomerate. The upper portion of this sequence is the host to gold skarn mineralization in the Nickel Plate deposit.

Deep water facies rocks ef the Stemwinder Mountain Formation form a 700 m thick succession of organic-rich, thinly bedded argillite, turbiditic siltstone, siliceous tuff and impure limestone. As the limestone beds seldom exceed 3 m in thickness, gold skarn mineralization in this unit is limited, occurring most notably at the Peggy mine (Fig. 1; Ettlinger and Ray, 1989).

All three sequences are conformably overlain by the Whistle Creek Tuff which represents the highest stratigraphic unit of the Nicola Group in the district. It consists of up to 1200 m of tuffaceous siltstone, andesitic ash and lapilli and minor volcanic breccia. Limestone is generally absent; however, an important marker horizon, the Copperfield conglomerate, lies at the base of the Whistle Creek sequence and contains abundant limestone fragments (Ray et al., 1987). The Copperfield conglomerate is interpreted to be an olistostrome by the authors.

Atleast three distinct suites of intrusive rocks are present in the Hedley district. The Hedley intrusions are the oldest suite, having been dated by U/Pb methods at 199 Ma. They form stocks greater than 1 km in diameter and swarms of dikes and sills up to 200 m thick (Ray et al, 1987). The stocks vary texturally and compositionally from the sills and dikes in that the stocks are generally equigranular and consist of biotite and hornblende granodiorite, quartz diorite, diorite or gabbro. Sills and dikes are porphyritic, range in composition from quartz diorite to diorite and minor gabbro and unlike the stocks, are spatially associated with gold skarn mineralization.

A second suite of intrusions consisting of coarse grained, massive biotie +/- hornblende granodiorite outcrops in the southeastern and northern portions of the

district (Fig. 1). Intrusion of the Cahill Creek pluton and Bromley batholith has resulted in hornfelsing of country rocks and local skarn development adjacent to the pluton but no occurrences of gold mineralization associated with this suite have been reported. The Cahill Creek pluton has been recently dated by U/Pb from zircon at 168 Ma.

The third intrusive suite consists of volumetrically insignificant feldspar porphyry dikes upto 3 m thick. They postdate skarn alteration and gold mineralization and while their age is uncertain, they may be related to the overlying dacitic volcaniclastic rocks of the Spences Bridge Group (Ray et al., 1988).

Whole rock and trace element geochemistry of both unaltered and altered Hedley intrusions are presented in Ray et al., 1988. They point out the sub-alkalic, calc-alkaline nature of the intrusions which are predominantly quartz diorites according to the normative classification of plutonic rocks by Streckeisen and Lemaitre (1979). Ettlinger and Ray (1988, 1989) describe intrusions from other gold-bearing skarn deposits in British Columbia and they also concluded that the majority of these intrusions are sub-alkalic, calc-alkaline and mafic in composition.

A comparison of the composition of the Hedley intrusions with plutonic suites from other ore deposits is illustrated in Figures 2A through 2D. An alkali-silica plot (Fig. 2a) shows that the Hedley intrusions fall into the island-aro field of porphyry-Cu related plutons. This comparison is also illustrated in Figure 2B, an alkali-CaO ternary diagram of porphyry-related plutons. Once again, the Hedley intrusions are lime-rich, and largely fall into the field of Pacific and Caribbean island-arc plutons (Titley and Beane, 1981). A comperison of normative mineralogy (Fig. 2C) shows that the Hedley intrusions are k-spar and quartz deficient compared to several porphyry-Cu intrusions and their normative mineralogy is most similar to intrusions associated with Fe-Au skarns in Alaska (Newberry and Swanson, 1986). Although it will be shown that the skarn mineralogy in the Niokel Plate deposit displays a similar reduced nature as W-

skarns, the Hedley intrusions are clearly distinct from granitoids related to scheelite skarns (Fig. 2D).

The ore bodies forming the Nickel Plate deposit are hosted by westerly dipping, gently folded calcareous and tuffaceous siltstones and limestones, intruded by a swarm of semi-conformable diortic sills and steeply dipping dikes (Billingsley and Hume, 1941; Ray et al., 1987). Figure 3 is a surface geologic map of Nickel Plate Mountain and shows the approximate location of the current minesite. Important features to note are the Toronto stock, which forms the largest mass of diorite on Nickel Plate Mt., and the "marble line" which is stratigraphically, the lowest limit to massive skarn replacement (Billingsley and Hume, 1941). This metasomatic boundary is almost entirely contained within a 90 m thick limestone unit historically known as the "Sunnyside limestone" (Camsell, 1910). The marble line forms a concave-upward, bowl shaped surface, which marks the boundary between pyroxene-garnet-sulfide skarn and underlying marble. Local, narrow projections of skarn occur below the marble line along steeply dipping, northwest trending dikes (Billingsley and Hume, 1941). The marble line is roughly concordant with the upper contact of the Sunnyside limestone, and dips westward with this unit, where it probably intersects the Toronto stock at depth (Fig. 4). Camsell (1910) first made the important observation that productive ore bodies in the Nickel Plate deposit are all located near the top of the Sunnyside limestone in the overlying thinly bedded sediments. Economic quantities of skarn hosted sulfide-gold mineralization are generally limited to within 100 m of the marble line (Ron Simpson, personal communication, 1987).

The uppermost limit of skarn alteration is less well defined, and probably not exposed in the mine cross section (Fig. 4) due to erosion. Ray et al. (1988) describes hornfelsic pyroxene, quartz and k-spar in the "upper siliceous beds" which overlie the Nickel Plate deposit. Alteration also extends into the Copperfield conglomerate which overlies the Hedley and Stemwinder Mt. Formations (Fig. 1).

Structural deformation in the Nickel Plate deposit is limited to gentle, small scale folds, district-wide recumbent folding and large scale reverse faulting. Rocks on Nickel Plate Mt. are part of the western limb of a north-northeasterly striking assymetric anticline with an overturned eastern limb. (Billingsley and Hume, 1941; Ray et al., 1988). Accompanying this district-wide folding are northerly trending high-angle reverse faults which typically juxtopose older, steeply dipping strata to the west, onto younger rocks to the east (Ray et al., 1988).

Small scale, northwesterly striking folds, formed early during emplacement of the Hedley intrusions, subsequently gave way to flat thrusts and fractures during the more brittle stage of skarn development (Billingsley and Hume, 1941). These structures are important local controls to ore formation particularly where clusters of folds and fractures intersect the Hedley sills.

Skarn Formation

Skarn alteration surrounding the Nickel Plate deposit encompasses a 6 square km. area up to 300 m thick and is the largest body of skarn in the district (Ray et al., 1988). Thinly bedded, calcareous and tuffaceous siltstones and limestones are the principle host to skarn formation. Complete replacement of the sediments by fine grained pyroxene and garnet (exoskarn) is common, and although few examples of remnant siltstone remain within the ore zone, primary sedimentary bedding is often preserved in the skarn. In comparison, alteration of the Hedley intrusions is widespread but not as intense as in the exoskarn. Pyroxene-garnet development in the dioritic sills and dikes (endoskarn) is only locally destructive of primary igneous textures. Variably altered remnants of diorite containing relic porphyritc texture and phenocryst cores of primary hornblende or plagioclase are common.

It is well documented that the Hedley intrusions acted as an essential component to formation of the gold skarn deposits in the district. Camsell (1910) first noted the close

association between economic ore bodies and the Hedley diorites, calling upon direct intrusion of these bodies resulting in a oontact metamorphio zone between the intrusion and surrounding sediments. More recently, Ray et al. (1988) described systematic geochemical changes as the result of progressive skarn development in the Hedley diorites and adjacent country rocks. However, whether the observed stocks, dikas and sills acted as the primary heat and fluid source; contributing base and precious metals to the exoskarn via an exsolved magmatic fluid is not certain.

Figure 4 is a cross section through the Nickel Plate deposit based on detailed logging of 1225 m of diamond drill core from 5 drill holes through the ore zone and 2 holes to the west, outside of this zone, towards the Toronto stock (Fig. 3). Correlation of sills from near the Toronto stock to the ore zone is highly interpretive due to the distances between these areas; however, an apparent increase in the volume of diorite intruding the section is observed in drill holes through the ore zone. Drill holes #514 and 413, located outside the main ore zone, 25m and 300rn respectively from the contact of the Toronto stock, averaged 25 percent Hedley diorite dikes and sills. In contrast, the five holes drilled through the ore zone averaged 39 percent diorite. This increase in diorite volume within the ore body is thought to be due to steeply dipping dikes which acted as feeders to some of the sills, a relationship first suggested by Billingsley and Hume (1941). This locus of dike and sill activity in the main ore zone is considered to be critically important in concentrating hydrothermal fluids and gold mineralization.

Endoskarn

The sills and dikes within the Niickel Plate ore body have undergone widespread alteration and replacement by skarn. Although this alteration sometimes results in the complete destruction of primary igneous minerals, the remnant igneous texture is often clearly preserved. Least altered examples of diorite exhibiting relic igneous amphibole

and augite phenocrysts are sometimes present as irregular patches in the center of thick sill units.

Development of endoskarn begins with early potassic alteration of hornblende and augite phenocrysts. Brown biotite replaces these minerals starting with their cores and increasing outward towards the phenocryst rim. Alteration of the plagioclase-rich matrix consists of fine grained quartz and up to 10 percent finely disseminated k-spar. Approximately 0.5 percent pyrrhotite and trace amounts of arsenopyrite are also present in the matrix and it is not clear whether these sulfides are primary components of the sills, as suggested by Camsell (1910), or introduced by later hydrothermal fluids during the alteration process. This early stage of alteration is rarely preserved and remains only in the cores of the thicker sill units. An example is illustrated in Figure 5a, a photomicrograph of remnant diorite from the inner portion of a thick sill near the top of hole #195 (Fig. 4).

Representative biotite analyses from the early potassic alteration are presented in Table 1. The phlogopite mole fraction, assuming all iron as Fe^{+2}, varies from 0.38-0.55. Corresponding weight percent TiO_2 values range from 0.5-1.8. The assumption that all iron in biotite is Fe^{+2} is reasonable because the corresponding number of Si+Al cations, based on 20 oxygen and 4 OH^-, ranges from 8.4-8.9. Thus there is an excess of 0.4-0.9 Al^{+3} cations to fill the biotite Y-site. Summing the possible Y-cations, Mg, Fe^{+2}, Ti and excess Al, gives a range of 5.5-6.1, indicating room for only minor amounts of Fe^{+3}. A comparison of these data with hydrothermal biotite from other ore systems is shown in Figure 6. The low phlogoplte and TiO_2 content of hydrothermal biotite from the Hedley sills compared to those from the Santa Rita porphyry copper deposit (Jacobs and Parry, 1979) and from potassic alteration associated with porphyry copper mineralization in the McCoy Creek district (Link, 1985) is an indication of the reduced nature of Nickel Plate mineralization compared to porphyry systems. This contrast is emphasized when it is considered that the McCoy

Creek pluton is interpreted to have been emplaced in an island-arc environment inboard of an active subduction zone (Link, 1985). This is the same depositional environment envisioned for the deposits of the Hedley district and other gold skarns in British Columbia (Ettlinger and Ray, 1989). Also shown for comparison in Figure 6 are analyses of biotite from the Kalzas wolframite vein deposit (Lynch, 1985), which like many Sn and W deposits, is interpreted as also having a reduced character compared to porphyry deposits such as Santa Rita.

With time, and progressing outward towards the sill margins, bleaching of the diorite results in a pale brown discoloration of the matrix; mafic phenocryst forms are still clearly visible. The early biotite and remaining hornblende and augite are replaced by either secondary amphibole of tremolite-actinolite composition or Mg-rich clinopyroxene (Tables 1 and 2, Fig. 5b). Alteration to pyroxene is by far the more common and it is the most diopsidic (Hd_{5-30}) found in endoskarn.

With increased hydrothermal activity, bleaching of the diorite is more pronounced in hand specimen and potassic alteration is more abundant. Early diopsidic pyroxene is replaced by k-spar and/or pyrrhotite. Although not abundant, thin pyroxene-k-spar-pyrrhotite veinlets appear to act as feeders, increasing the amount of potassic alteration until up to 90 percent of the phenocrysts and 60 percent of the matrix is replaced by k-spar (Fig. 5c). The pyroxene present in veins with k-spar and pyrrhotite is clearly later and more hedenbergitic (Table 2 and Fig. 7) than the early pyroxene replacing the mafic phenocrysts.

Alteration in the sills is most intense along their contacts with exoskarn. The diorite is bleached white with no mafic phenocrysts remaining. These rocks have undergone extensive Ca-Na metasomatism with up to 80 percent of the rock replaced by plagioclase (An_{24-52}, Table 1). Pyroxene remains only as a skeletal framework outlining the relic phenocryst form and sphene occurs as an important alteration mineral. Pyrrhotite and chalcopyrite are present in only trace amounts.

Replacement of diorite by massive pyroxene-garnet skarn overprints the above alteration sequence and may result in complete destruction of original igneous textures (Fig. 5d). This pyroxene ranges in composition from Hd_{47-83} and is compositionally distinct from the earlier diopsidic and vein controlled pyroxenes (Table 2, Fig. 7). However, this massive skarn is texturally and compositionally similar to the bulk of exoskarn (Fig. 8b), and when developed, makes it difficult to identify the original protolith.

Exoskarn

Skarn formation in the Nickel Plate deposit begins with early, isochemical recrystallization of sediments and limestone and evolves through time into the complete metasomatic replacement of the protolith by calc-silicate and sulfide minerals, the final bulk chemistry of the skarn being distinctly different from the original protolith composition. However, as pointed out by Einaudi et al. (1981), it is impossible to clearly separate these two endmember processes; thus, in the Nickel Plate deposit a continuum probably exists between purely isochemical and purely metasomatic events.

The earliest changes observed in Hedley Formation sediments involves recrystallization of siltstone and limestone members to fine grained siliceous hornfels and marble repectively. In thin section, the hornfelsed siltstones consist of irregular, <5 micron size grains of quartz and potassium feldspar with thin laminae of recrystallized calcite defining remnant carbonate-rich lenses. Remnant patches of this hornfels are present throughout the deposit; however, they appear to be most abundant near the upper margin of skarn formation. Thicker limestone members consist of recrystallized calcite exhibiting metamorphic triple junction grain boundaries. This stage of hornfelsing and recrystallization is believed to be approximately coeval with initial emplacement of the Hedley intrusions.

The formation of biotite and clinopyroxene hornfels and skarnoid follows recrystallization of the sediments. This process involves only local (centimeter scale) exchanges in cations through circulation of an intergranular fluid. Skarnoid development begins with alteration of the siliceous hornfels by reddish-brown biotite occuring as finely disseminated grains and coarser clots which are fed by 5-10 micron wide biotite veinlets. A similar biotite alteration style occurs at the Frenoh mine, 5 km south of Nickel Plate (Fig. 1), where fracture controlled biotite hornfels appears as a halo surrounding calc-silicate skarn.

A second stage of skarnoid is represented by the first occurrence of clinopyroxene in the sediments. It is fine grained and varies from being unevenly disseminated throughout the sediments where it forms <10 percent of the rock, to being the most abundant mineral present occurring in anhedral crystal aggregates replacing up to 90 percent of the sediment. This early pyroxene ranges in composition from Hd_{48-59} (Table 2, Fig. 8b). Early, diopsidic pyroxene is also observed as isolated grains in marble beyond the marble line and like the skarnoid pyroxene, is believed to be caused by limited, early fluid flow in response to thermal gradients established through emplacement of the Hedley intrusions.

Skamoid is gradational into purely metasomatic calc-silicate alteration characterized by pyroxene-rich skarn. The early, generally sparsely disseminated skarnoid pyroxene gives way to massive skarn, with the sediments and early skarnoid being replaced by more hedenbergitic pyroxene (Table 2). As this iron-rich pyroxene continues to overgrow remaining hornfels and skarnoid, garnet begins to crystallize. Early garnet forms anhedral masses up to one centimeter in diameter and contains numerous inclusions of earlier pyroxene. Both isotropic and anisotropic garnet are present. The majority of garnets in the Nickel Plate deposit are grossularitic in composition but range from Ad_{14-82} and average Ad_{35} (Table 3, Fig. 8a); compositions of Ad_{73-82} are limited to the ore zone.

With time, the amount of garnet in the skarn shows a minor increase relative to pyroxene. Garnet becomes coarser grained, more birefringent and exhibits complex sector and concentric zonation patterns which do not show any consistent compositional trends. The resulting pyroxene-garnet skarn is often strongly banded, with the coarser garnet bands replacing carbonate-rich layers, while the pyroxene favors the clastic-rich zones. Typical ore grade skarn at Nickel Plate is fine grained, dark green in hand specimen and consists largely of hedenbergitic pyroxene with visible arsenopyrite.

Secondary minerals associated with the main stage of pyroxene-garnet skarn include quartz, calcite, k-spar, apatite, plagioclase, sphene, pyrrhotite, pyrite, arsenopyrite and ilmenite. The quartz and k-spar occur predominantly in narrow (<20 microns) skarn veins with pyroxene which crosscut earlier skarnoid and poikolitic garnet but appear contemporaneous with the main deposition of massive pyroxene-garnet skarn. Apatite occurs most often as euhedral grains disseminated in skarn hosted by carbonate-rich protolith. Plagioclase and sphene are minor, fine grained components of the skarn.

At the marble line (Fig. 9), the outer most extent of calc-silicate skarn is marked by silicification of marble that may extend several meters away from the skarn contact as irregular pods of fine grained quartz resembling a siliceous hornfels.

Silicification also occurs well beyond the marble line where diorite sills cross cut the underlying limestone. Disseminated within this marble are minor amounts of ilmenite and rutile. The carbonate is completely recrystallized and partially replaced by quartz. Chlorite, calcite, wollastonite and sulfides, consisting of arsenopyrite, pyrrhotite and chalcopyrite, replace the quartz.

Coarse potassium feldspar is also noted in the lower portion of the skarn zone, most abundant near the marble line where it occurs with calcite and quartz and is later than pyroxene and garnet skarn. Silicification and potassium feldspar alteration is also

reported in the "upper siliceous beds" overlying the Nickel Plate deposit where the host is predominantly thinly bedded crystal tuffs and clastic-rich sediments (Ray et al., 1988).

Retrograde alteration of pyroxene-garnet skarn to a lower temperature, hydrous silicate assemblage is not significant in the Nickel Plate deposit. Ferroan-wollastonite, containing up to 5.09 wt percent FeO (Table 3) appears to be associated with the latest stage of massive skarn where it occurs in fibrous clusters replacing minor amounts of garnet and pyroxene in both diorite and exoskarn. Locally, massive epidote replaces endoskarn, as in the steeply dipping South dike (Fig. 9), which contains approximately 70 percent epidote replacing phenocrysts and matrix. Calcite, quartz, prehnite, clinozoisite, rutile and chlorite are also present in minor to trace amounts as late cross cutting veinlets and alteration products of pyroxene and garnet. However, the limited nature of this alteration compared to gold skarn deposits near porphyry systems (e. g. Fortitude and McCoy NV, Myers and Meinert, 1989; Brooks, et al., *in preparation*) and the copper skarns at Whitehorse, YT (Meinert, 1986), separates the Nickel Plate deposit from those skarns exhibiting significant retrograde alteration.

Scapolite

Scapolite is found in varying quantities throughout the deposit as an alteration product of plagioclase phenocrysts in the sills, with gold-sulfide mineralization in ore zone exoskarn and as subhedral poikolitic crystals in marble beyond the outer limits of skarn formation. Dolmage and Brown (1945) report that scapolite in the prophyry sills is Na-rich (dipyre, $Marialite_{73}$- $Meionite_{27}$) which suggests this alteration could have resulted from Na-Cl metasomatism of intermediate plagioclase. Ray et al. (1986) report a more calcic variety, mizzonite, as solution cavity fillings in the Copperfield conglomerate which immediately overlies the Hedley Formation.

Qualitative energy dispersive X-ray analysis (Kevex) of scapolite from marble underlying the ore zone indicates a more meionitic composition with a relatively low Na/Ca ratio. Scapolite is also reported in marble at the Duchess mine in the Cloncurry district of northwestern Queensland, Australia (Edwards and Baker, 1954), but there it has a diapyric composition. It is associated with a sequence of scapolite-pyroxene granulites formed through Na-metasomatism of calcareous shales during regional metamorphism. The authors concluded that in the Cloncurry district, the formation of Na-rich scapolite in marble rather than Ca-rich scapolite, which would be expected, was a function of Al activity because of the coupled substitution of Na^{+1}-Si^{+4}=Ca^{+2}-Al^{+3}. Along these lines, the Ca-rich scapolite found in marble at Nickel Plate could be the result of abundant Al released by the Ca-Na alteration in endoskarn sill margins.

Sulfide mineralogy and ore formation

Sulfides and related gold mineralization in the Nickel Plate ore body are often accompanied by scapolite deposition, all of which continue past the main period of pyroxene-garnet skarn formation. Although sulfides were also deposited prior to and after this main period of gold deposition, they are not generally abundant and except for some isolated massive occurrences, are usually not present in quantities greater than 5-7 percent.

The sulfides present in decreasing order of abundance are: arsenopyrite, pyrrhotite, chalcopyrite, pyrite, sphalerite, hedleyite, native bismuth, gold, galena, maldonite (Au_2Bi) and loellingite. Arsenopyrite is economically the most important sulfide present, occurring both prior to, and directly associated with gold deposition. Camsell (1910) reports its distribution is widespread, being found in all igneous rocks of the district, in sediments near intrusive contacts and as a primary constituent in volcanic rocks of the Red Mountain (Whistle Creek) Formation. He describes two generations of arsenopyrite; the later being less crystalline, having a bluish tint and "more often an

indication of good gold values than the well crystallized forms". Early arsenopyrite appears as euhedral rhombs up to 1-2 mm long and is associated with pyrrhotite and trace amounts of chalcopyrite in endoskarn. In sediments, the above association is not as strong, as it commonly occurs as isolated rhombs poikolitically enclosing remnant siltstone and early skarnoid pyroxene.

Mineralization occurs in all rock types in the Hedley district but is most abundant and highest grade in pyroxene-dominant skarn. The main stage of gold deposition is often characterized by coarse grained scapolite and arsenopyrite which contains inclusions of pyrrhotite, chalcopyrite, Bi-tellurides, gold and galena. The scapolite, which comprises <10 percent of the ore-bearing skarn, forms coarse anhedral masses enclosing pyroxene and garnet in exoskarn, but is finer grained and preferentially replaces plagioclase phenocrysts in the endoskarn. Arsenopyrite, in contrast to its earlier occurrence, is not poikolitic and anhedral forms are most common. It contains up to 0.73 wt percent Bi and 4.15 wt percent Co (Table 4). Bismuth-telluride mineralization occurs as inclusions of hedleyite, native bismuth, and maldonite. In polished section, visible gold grains up to 35 microns across always occur with hedleyite, both as inclusions or as fracture fillings in arsenopyrite. Gold or hedleyite surrounded by calc-silicate gangue without sulfides is exceedingly rare. Gold fineness ranges from 770-860 (Table 4).

Pyrrhotite appears to be the only significant sulfide to be deposited after the main period of gold deposition. It occurs in late cross cutting veinlets with prehnite and petrograhic evidence suggests this late pyrrhotite replaces pyroxene, arsenopyrite and chalcopyrite.

Skarn zonation

Skarn in the Nickel Plate deposit is distinctly zoned in terms of: 1) garnet and pyroxene abundance; and 2) pyroxene composition; and shows only a weak zonation

in garnet composition. Garnet is most abundant adjacent to the eastern margin of the Toronto Stock where it constitutes almost 50 percent of the skarn (Figs. 9 and 10). This results in an average garnet/pyroxene ratio of about 1.1:1, with local, calcite-rich sediments containing garnet/pyroxene ratios greater than 10:1. Eastward towards the ore zone, the garnet/proxene ratio rapidly decreases to less than 1:5, with areas of almost pure pyroxene skarn occurring in the upper portion of the drill holes furthest to the east.

Variation in garnet and pyroxene composition across the deposit is illustrated in Figure 11. Garnet shows a decrease in andradite content adjacent to the Toronto stock and in drill hole #262 on the eastern margin of the ore zone. Garnet therefore, is zoned about the South dike feeder zone and becomes Mn-rich and more aluminous both proximal to the Toronto stock and near the outer margin of the skarn envelope (Figs. 4 and 11).

Iron content of pyroxene from exoskarn is relatively constant from the Toronto stock to the western margin of the ore zone, averaging about Hd_{52} (Fig. 11). East of the South dike the iron content increases sharply to Hd_{73} in drill hole #262. Thus as in garnet, pyroxene shows a compositional zonation relative to the South dike feeder zone exhibiting proximal Mg, and distal Mn+Fe-enrichment.

Summary

Skarn deposition in the Nickel Plate deposit is preceeded by isochemical recrystallization of siltstone and marble. Biotite and pyroxene hornfels and skarnoid follows and overprints this early metamorphic recrystallization. Intrusive rocks are potassically altered and only display Mg-rich pyroxene replacement of mafic phenocrysts during this early period of alteration.

The main stage of skarn formation is characterized by dark green, Fe-rich pyroxene skarn, lesser aluminous garnet, arsenopyrite and pyrrhotite; this main stage replaces all earlier alteration, often resulting in complete destruction of original rock texture.

Sulfide deposition continues past the main period of calc-silicate skarn formation. Gold is most abundant in pyroxene-rich exoskarn and is intimately associated with arsenopyrite and Bi-telluride mineralization. Coarse scapolite often accompanies the arsenopyrite-Au mineralization.

The widespread occurrence of scapolite in the Nickel Plate deposit is unusual in skarn deposits. One explanation may relate the scapolite to the Ca-Na metasomatism of diorite in the sill margins. The addition of Na to plagioclase would release Al, which under favorable conditions would react with Ca in the hydrothermal fluids to form scapolite.

An approximate correlation of time equivalent alteration stages between the dioritio sills and dikes of the Hedley intrusions and the sedimentary rocks of the Hedley Formation is summarized in Table 5. The spatial relationships of these alteration stages is shown in Figure 12. A comparison of the compositional and temporal relationships between endoskarn and exoskarn alteration indicates that these two skarn types are quite similar in their gross mineralogy and alteration sequence. This may be the result of overprinting of diorite and sedimentary rock by a fluid-rich hydrothermal system which evolved later than, and independantly of crystallization of the Hedley sills and dikes.

Fluid Inclusion Study

Analyses of fluid inclusions in skarn samples from different locations in the Nickel Plate ore body were .used to estimate the temperature and salinity of the skarn forming fluids.

Homogenization and freezing temperatures were determined using a Fluid Inc. modified, U.S.G.S. gas flow heating/cooling stage. Sample preparation and calibration techniques and stage accuracy are described by Meinert (1984, 1987).

Fluid inclusions from garnet, clinopyroxene, quartz and scapolite were analyzed. Discrimination of primary versus secondary fluid inclusions followed the recognition

criteria of Roedder (1984). In contrast to many base metal skarns (Kwak, 1986), primary fluid inclusions are not abundant in the Nickel Plate skarn and when present, are generally less than 10 microns in diameter. Clinopyroxene contained the most suitable inclusions for study, averaging 8 microns in diameter. They commonly occur as single, isolated inclusions with a 1 cm X 1 cm chip often yielding only one or two inclusions. Planar arrays of secondary inclusions are not present. In contrast, garnet contained numerous secondary inclusions making the identification of primary inclusions difficult. Inclusions in garnet also averaged less than 10 microns in diameter but owing to the coarser habit of garnet compared to clinopyroxene, multiple inclusions were found in individual garnet crystals.

The majority of the inclusions in garnet and clinopyroxene are two phase liquid + vapor with an average vapor fill volume of 23 percent. All inclusions in clinopyroxene and garnet homogenized to a liquid upon heating, whereas in quartz, some inclusions homogenized to a vapor. No conclusive evidence for fluid boiling was found. Many inclusions decrepitated prior to reaching their homogenization temperature; data for these inclusions are only reported when shrinkage of the vapor bubble was sufficient to suggest homogenization would occur within 20-30^{o}C of the decrepitation temperature.

Daughter minerals are present in <10 percent of the inclusions. Three types of daughters are observed, the most common occurring as subhedral tabular grains with high birefringence is tentatively identified as nahcolite (Shepherd et. al., 1985). Although rare, halite was identified in clinopyroxene, garnet and quartz. Additionally, opaque daughters, too small for optical identification are found in clinopyroxene and scapolite.

All primary fluid inclusions homogenized over a temperature range of 210-730^{o}C (Figs. 13A, 13B and 13C). Mean homogenization temperatures for garnet and clinopyroxene (Figs. 13A and 13B) are 384 and 368^{o}C respectively. The highest

homogenization temperatures (720-730^{o}C) are from garnet in the lower portion of hole #514 which is adjacent to the Toronto Stock (Fig. 4). Homogenization temperatures up to 695^{o}C also occur in clinopyroxene from the bottom of hole #378, from exoskarn formed in the footwall of the South dike.

Fluid inclusions in quartz homogenized between 320-540^{o}C and showed a systematic decrease in temperature away from the Toronto Stock eastward to the edge of the ore zone (Fig. 13C). Average homogenization temperatures from quartz replacing marble at the marble line ranged from 514^{o}C in the bottom of hole #514, to 398^{o}C in the bottom of hole #135 and 351^{o}C in the bottom of hole #262.

Scapolite showed the lowest average homogenization temperature (347.5^{o}C), homogenizing in the range 320-400^{o}C (Fig. 13C).

Fluid salinity was estimated from last ice melting temperatures using the equations of Sterner et al. (1988). Nine inclusions in garnet and clinopyroxene yielded suitable optical characteristics to make this measurment. The remaining inclusions either were too small to view ice melting or showed no sign of freezing down to -175^{o}C. In garnet, temperature of last melting of ice ranged from -24 to -4.2^{o}C with an average of -16.1^{o}C, while in pyroxene the range was -9.5 to -2.5^{o}C with an average of -6.6^{o}C. This corresponds to an average salinity of 18.3 and 9.7 wt percent NaCl equivalent, respectively.

The rare presence of halite daughters in clinopyroxene and quartz indicates the skarn forming fluids contained greater than 26.2 wt percent NaCl equivalent for at least a part of their evolutionary history. This is supported by the low range of last melting of ice in garnet (-24^{o}C) which also indicates NaCl saturation at standard conditions (25^{o}C, 1 bar). The temperature at which the halite daughters dissolve upon heating can be used to estimate total fluid salinity using the equation of Potter et al. (1977). For halite-bearing inclusions in pyroxene and quartz from skarn, measured dissolution temperatures were 216^{o}C and 296^{o}C, respectively. This results in a total fluid salinity

of 32.7 wt percent NaCl equivalent in pyroxene and 37.9 wt percent NaCl equivalent in quartz.

The depth of skarn formation in the Hedley district is not well constrained. A general lack of brecciation and veining in the skarn and an absence of near surface volcanic expression of the Hedley intrusions suggest a depth >3 km (Burnham and Ohmoto, 1980). Conversely, the inequigranular, weakly porphyritic texture of the sills and the lack of high temperature/pressure metamorphism of Hedley Formation sediments precludes a deep level of skarn formation such as the 7-15 km estimated for some W-skarns (Newberry, 1982). These general geologic constraints suggest an intermediate depth of skarn formation between 3 and 7 km. Therefore, in order to estimate the approximate pressure of skarn formation, a depth of 5 km for the Nickel Plate skarn deposit is assumed. Using a density of 2.70 gcm^{-3} for lithostatic overburden and 1.00 gcm^{-3} for hydrostatic head, a maximum (lithostatic) pressure of 1324 bars and a minimum (hydrostatic) pressure of 491 bars is estimated. The prevailing pressure at the time of skarn formation was probably closer to lithostatic pressure due to the features described above. Therefore, a value of 1 kbar is considered a close approximation of the pressure during skarn formation. Using this estimated pressure, the temperature correction diagrams of Potter et al. (1977) yield temperature corrections of 95 and 98°C for fluid inclusions in garnet and pyroxene, respectively. This places the average temperature of formation for pyroxene-garnet skarn between 460-480°C and the highest temperatures in the range of 700-800°C.

Discussion

The different styles of alteration present in the Nickel Plate deposit exhibit systematic variations in mineralogy and geochemistry. However, extensive overprinting of multiple protoliths along with the numerous fluid channels offered by the many sills, dikes and stocks present in the Hedley district, results in an alteration

pattern which is not as strongly or uniformly zoned as some other base and precious metal skarns described in the literature (Groundhog Zn-Pb deposit, Meinert, 1987; Fortitude Au deposit, Myers and Meinert, 1989; Carr Fork Cu-Au deposit, Atkinson and Einaudi, 1978, Cameron and Garmoe 1987; and MacTung W-Cu deposit, Dick and Hodgson, 1982). Nonetheless, the spatial, temporal and geochemical variations can be used to construct a model illustrating the evolution of skarn and gold mineralization at Nickel Plate.

Skarn mineralogy and zonation

The large amounts of hedenbergitic pyroxene and subordinate amounts of grossularitic garnet that form exoskarn in the Nickel Plate ore body were deposited under more reduced conditions than typically found in skarns related to porphyry-Cu systems. This is illustrated in Figure 14 (modified from Einaudi, 1982) which shows the compositional range and average values for pyroxene and garnet from exoskarn in the Nickel plate ore zone. Garnet and pyroxene from Nickel Plate are clearly distinct from garnet and pyroxene found in porphyry-Cu skarns and plot in the reduced region characterized by Sn+W-skarns (Einaudi, 1982). An important feature of Sn+W-skarns is their reduced calc-silicate and sulfide mineral assemblages which clearly separate them from Cu-, Fe- and Zn-Pb skarns (Einaudi et al., 1981).

The overall trend of Nickel Plate skarn mineral zonation is centered on the locus of diorite dikes, such as the South dike, in the ore zone. As was illustrated in Figure 11, pyroxene becomes more manganese, and iron-rich and garnet becomes more aluminous away from this skarn center in the ore zone. This zonation pattern is thought to reflect the dominant flow pattern of hydrothermal fluids. This pattern contrasts sharply with the progressive decrease in garnet-pyroxene ratio away from the Toronto stock (Fig. 10). A general decrease in garnet-pyroxene ratio away from a central pluton occurs in most skarn systems and is thought to reflect overall

temperature/metasomatic gradients (Einaudi, et al. 1981). These skarn mineral zonation patterns in the Nickel Plate deposit suggest that there were two dominant paths of fluid flow: one outward from the Toronto stock along permeable horizons and diorite sill contacts, and a second outward from the locus of dikes, such as the South dike, in the ore zone. Further evidence for complex fluid flow paths is provided by spatial correlation trends of skarn mineral compositions.

Pyroxene from the ore zone in the Nickel Plate deposit exhibits a correlation between iron and manganese content which is different from pyroxene nearer the Toronto stock, outside the ore zone (Fig. 15). Manganese enrichment in ore zone pyroxene is proportional to the hedenbergite content, a trend which can be approximated by the relationship: mole percent Jo=0.04 x mole percent Hd + 0.4. In contrast, manganese content in the majority of pyroxene from outside the ore zone (drill hole #514 and #413, Figs. 4 and 15), is higher overall and inversely proportional to the hedenbergite content. The enrichment of iron and manganese in pyroxene from the distal parts of a skarn system has been reported for many different skarn types (e.g. Cu skarns - Cananea, Mexico, Meinert, 1982; Fe skarns - Vancouver Island, British Columbia, Meinert, 1984; Zn-Pb skarns - Groundhog, New Mexico, Meinert, 1987), however the increase in manganese with a decrease in iron as observed in the Nickel Plate system outside the ore zone, is fairly unusual.

Garnet compositions are more variable than pyroxene but still suggest two separate skarn mineral populations. In contrast to pyroxene, the manganese content of garnet from the ore zone is inversely proportional to the iron content (mole % Py=-0.01Ad + 1.5). The negative correlation between manganese and iron is less strong in garnets from outside the ore zone (Fig. 16). These two discreete skarn mineral populations, one in the ore zone and one distal to the ore zone, are thought to result from independent fluid flow paths because there are no significant systematic differences between the skarn protoliths. Changes in the oxidation/sulfidation state could explain

some of the partitioning of Fe-Mn between garnet and pyroxene but not the reversal in composition trends observed between the different parts of the deposit. Further evidence for multiple fluid flow paths in the Nickel Plate skarn system will be presented later in the sections on fluid inclusion and sulfide mineralogy.

Fluid inclusion data

Fluid inclusion homogenization temperatures in pyroxene and garnet suggest that the skarn-forming hyrdrothermal fluids were dispersed from two separate locations that are currently represented by homogenization temperature highs. This is illustrated in Figures 17a and 17b whioh are contoured cross sections of average fluid inclusion homogenization temperatures in garnet and pyroxene, respectively. A locus of high homogenization temperatures in garnet are found in hole #514 adjacent to the Toronto stock; whereas, the highest average temperatures in pyroxene are from the bottom of hole #378, at the intersection of a thick sill and the South dike (Fig. 17b).

Average homogenization temperatures in pyroxene appear to increase with depth (Fig. 18). However, no systematic variation in pyroxene homogenization temperatures with distance from the nearest sill has been observed. These observations along with the high homogenization temperatures in ore zone pyroxene and from garnet near the Toronto stock, suggest that the bulk of skarn forming fluids originated at depth and were channeled along dike contacts in the ore zone and along the margin of the Toronto stock to the west, rather than directly from the dikes and sills themselves. This is consistent with: 1) the large amount of skarn formed from sills and dikes, 2) the high garnet/pyroxene ratios found nearer the stock, and 3) the Mn-enrichment observed in pyroxene both at the stock contact and in the ore zone, near the marble line (*see* Fig. 23).

Geochemistry

An estimate of oxygen and sulfur fugacities during the main period of Fe-rich pyroxene skarn deposition is shown in Figure 19. The stability fields of major calc-silicate and sulfide minerals are drawn at 500°C and XCO_2=0.1. The common occurrence of hedenbergitic pyroxene, pyrrhotite and arsenopyrite, and the absence of the assemblage andradite-quartz pyrrhotite in the Nickel plate deposit limits log fS_2 to the range -6.5 to -7.8. The range of oxygen fugacity is limited by the abundance of pyrrhotite with hedenbergitic pyroxene skarn and the near absence of magnetite and graphite resulting in a log fO_2 of approximately -22 to -25. The stability field of the hedenbergitic skarn in the Nickel Plate deposit is shown as the cross-hatched area in Figure 19.

A general increase in the Fe-content of pyrrhotite occurs from west to east across the deposit (Fig. 20a). The sporadic association of pyrite with pyrrhotite indicates that formation of these two minerals in the Nickel Plate deposit occurred at aS_2 and T conditions which at least in part, defines the pyrite + pyrrhotite univariant curve shown in Figure 20b. Also shown is a cooling path from higher temperature, low-Fe pyrrhotite found nearer the Toronto stock (point A), to lower temperature, high-Fe pyrrhotite, occurring distal to the stock near the marble line (point B). This indicates fluids from which pyrrhotite and pyrite were deposited, had an average temperature range and sulfur activity of 600-650°C and log aS_2=-2 proximal to the Toronto stock and <400°C and log aS_2=-7 to -8 at the marble line.

The high average temperatures obtained from pyrrhotite oomposition near the Toronto stock correspond well with fluid inclusion homogenization temperatures of up to 730°C in garnet from the same area. Within the ore zone, homogenization temperatures of up to 695°C occur in pyroxene; while the highest average temperature estimated by pyrrhotite composition is in excess of 500°C (Hole #135, Fig. 20b). Thus, fluid inclusion homogenization temperatures are consistent with

temperatures calculated from pyrrhotite composition, especially when it is considered that the pyrrhotite temperatures are averages for each drill hole, individual pyrrhotite analyses as low as 45.0 atom percent Fe within the ore zone and adjacent to the Toronto stock indicates temperatures of pyrrhotite deposition in excess of 700^{o}C for these areas.

Hedleyite, gold, bismuth, and maldonite commonly occur together as inclusions in arsenopyrite and are found only within skarn in the ore zone (Fig. 9). The presence of hedleyite indicates a maximum temperature of last equilibration for this assemblage of 312^{o}C; while the separation of maldonite into its low temperature assemblage, Au + Bi, indicates that part of this mineralization continued to as low as 113^{o}C (Barton and Skinner, 1979). A temperature range of 113-312^{o}C for Au-Bi mineralization is lower than that estimated for arsenopyrite deposition. This is illustrated in Figure 21, a log aS_2-T diagram, showing the stability field of arsenopyrite and the variation in arsenic content with T and sulfur activity. Arsenopyrite contains between 32.7 and 35.9 atom percent As indicating an approximate temperature range of 400-550^{o}C for this mineralization. In the ore zone, arsenopyrite has a higher arsenic content than arsenopyrite in drill holes #514 and 413 nearer the Toronto stock, which reflects a slightly higher temperatures during the main period of sulfide deposition (Fig. 21). Sulfur activity for the range of arsenopyrite compositions plotted in Figure 20 varies from -4 to -10 log aS_2, which is also approximately the same range for pyrrhotite deposition below 500^{o}C (Fig. 20B). Accordingly, the majority of arsenopyrite was deposited under similar conditions of T and sulfur activity as at least some of the massive pyroxene skarn.

Petrographic evidence indicates that the bulk of Au-Bi mineralization is contemporaneous with arsenopyrite deposition; whereas, mineral stability relationships indicate the Au-Bi mineralization equilibrated at temperatures 200-400^{o}C below those for arsenopyrite. Therefore, Au-Bi mineralization was probably

precipitated from the hydrothermal fluid during the main period of pyroxene-arsenopyrite deposition, being contained as lattice constituents of the arsenopyrite at elevated temperatures. As the system cooled, the hedleyite, gold and bismuth exsolved from the arsenopyrite at temperatures approximately below 312^{o}C.

A range of sulfur activity for Au-Bi mineralization can be estimated using the sulfide mineral stability fields shown on the log fO_2-log fS_2 diagram for T=300^{o}C in Figure 22. The presence of native bismuth rather than bismuthinite, and minor amounts of pyrite with pyrrhotite, places an approximate upper limit on this mineralization log fS_2= -10. A lower limit of log fS_2=-15 can be further estimated by the dominance of arsenopyrite over the assemblage pyrrhotite+loellingite.

Summary and Conclusions

The Nickel Plate gold skarn deposit is characterized by hedenbergite pyroxene, aluminous garnet, arsenopyrite, and Au-Bi-telluride mineralization which overprints earlier recrystallized sediments and biotite and pyroxene skarnoid. The bulk of the pyroxene-rich skarn formed in the temperature range of 375-575^{o}C (pressure corrected) with temperatures locally as high as 700-800^{o}C. This indicates the Nickel Plate deposit formed at temperatures moderately higher than observed at ferrous and base metal skarns (Kwak, 1986; Meinert, 1984, Einaudi et al., 1981). The temperatures encountered at Nickel Plate may also be higher than those found at other gold skarn deposits (Myers and Meinert, 1989; Torrey, 1986) although the amount of fluid inclusien data available from these deposits is very limited.

Mineral stability relationships indicate that the hedenbergite skarn formed under a log fS_2 range of -7.8 to -6.5 and a log fO_2 of -25 to -22. A similar temperature range of 450-550^{o}C and log fS_2 of -10 to -4 is estimated for arsenopyrite deposition based on compositional data. Variations in pyrrhotite compostion yield an average temperature for this mineralization of 600-650^{o}C and log aS_2= -2 proximal to the Toronto stock,

and temperatures <400^{o}C and log aS_2= -7 to -8 at the marble line. The Au-hedleyite-Bi ore assemblage indicatos a temperature range of 113-312^{o}C and log fS_2 of -15 to -10. Petrographic evidence suggests the Au-Bi-Te mineralization was deposited with the arsenopyrite, possibly as a lattice constituent, and equilibrated to its current assemblage with falling temperatures. Thus it appears that the bulk of pyroxene-garnet-pyrrhotite-arsenopyrite skarn formed above 375^{o}C, whereas the Au-Bi-Te ore minerals last equilibrated, or possibly first precipitated, below this temperature.

The close association of arsenopyrite, gold and Bi-telluride mineralization in the Nickel Plate deposit as well as that reported from other gold skarns (Torre, 1986; Meinert, 1988; Kuyper, 1988; Myers and Meinert, 1989; Ettlinger and Ray, 1989) separate these deposits from base and ferrous metal skarns. However, the large amounts of pyrrhotite and notable absence of iron oxides at Nickel Plate suggests this deposit experienced more reducing conditions than most other gold skarns.

Mineralogical, geochemical and fluid inclusion data from Nickel Plate indicates the presence of two primary channels for dispersion of hydrothermal fluids originating at depth (Fig. 23). The eastern contact of the Toronto stock acted as one of these fluid conduits resulting in high garnet/pyroxene ratios, high homogenization temperatures and Al-enrichment in garnet proximal to the stock, and the progressive decrease in temperature away from the stock as indicated by pyrrhotite composition.

A second channel for the skarn-forming fluids occurred near the ore zone along the margin of steeply dipping dikes, most notably the South dike. An apparent thickening of sills in the ore zone and an increase in the percentage of diorite making up the stratigraphic section there, suggests this South dike also acted as a major feeder to the Hedley sills. Fluid flow along these dikes resulted in the observed high homogenization temperatures in pyroxene, Mn-enrichment in pyroxene east and west of this dike, and the sharp rise in Fe-content of pyroxene towards the eastern margin of the ore body. Two populations of pyroxene displaying different Jo/Hd ratios and

Mn-contents are probably also the result of skarn deposition from fluids migrating from these two fluid conduits.

Gold skarns, as a class of ore deposit, are becoming increasingly important as high grade sources of gold (Meinert, 1988). Based upon this study, the first of a major producing gold skarn, the most important exploration features of a Hedley-type system are:

1) Clastic-rich sedimentary sequence deposited in an oceanic back-arc environment. A reduced wall rock assemblage containing organic-rich, thinly interbedded limestones with tuffaceous and calcareous siltstone or argillite, is most favorable.

2) Small mafic bodies of sub-alkalic, calc-alkaline quartz diorite and diorite which form porphyritic sill/dike swarms and/or equigranular plug-like bodies.

3) Early hornfelsing and development of skarnoid in the sedimentary protolith. This may consist of biotite, k-spar, Mg-rich pyroxene or quartz hornfels which with time, evolves into extensive replacement of sedimentary and igneous rocks by skarn.

4) Skarn consists dominantly of hedenbergitic pyroxene with lesser grandite garnet, and subordinate amounts of scapolite, calcite, wollastonite, k-spar, quartz, biotite, prehnite, apatite, sphene, plagioclase, epidote, rutile, clinozoisite and chlorite. A reduced, low total-sulfur ore bearing assemblage consisting of one or more of the following: arsenopyrite-pyrrhotite-Bi tellurides-Au-native Bi. Large amounts of sulfides are not required.

5) Moderate to high fluid salinities (10 - >25 wt % NaCl equivalent) and high fluid inclusion homogenization tmeperatures (400-700^{o}C) in pyroxene and garnet skarn.

6) Although the number of different skarn minerals present is relatively small, a complex mineral distribution and geochemical zonation pattern results from dispersion of hydrothermal fluids along numerous intrusive and sedimentary contacts, and skarn replacement of a stratigraphically complex protolith.

Acknowledgements

The authors wish to gratefully acknowledge the financial and logistical support supplied by Mascot Gold Mines Ltd. Grants from Falconbridge Ltd.; the National Science Foundation (EAR-8814968); the Washington Mining and Mineral Resources Research Institute; Sigma Xi; and the Womens Auxillary of the American Institute of Mining Engineers helped support analytical and fieldwork. Scott Cornelius, Diane Johnson and Charles Knaack of the Electron Beam Microanalysis Laboratory, Dept. of Geology, Washington State University, deserve special thanks for their assistance during microprobe analyses. Aka and Kalaika provided crucial field assistance.

References

Atkinson, W.W., Jr., and Einaudi, M.T., 1978, Skarn formation and mineralization in the contact aureole at Carr Fork, Bingham, Utah: Econ. Geol. v. 73, p. 1326-1365.

Barr, D.A., Fox, P.E., Northcote, K.E., and Preto, V.A., 1976, The alkaline suite porphyry deposits-a summary: Canadian Inst. of Mining and Metallurgy, P. 36, p. 359-367.

Barton, P. B., Jr., and Skinner, B. J., 1979, Sulfide mineral stabilities, *in* Barnes, H. L., ed., Geochemistry of hydrothermal ore deposits: New York, Wiley Intersci., p. 278-403.

Billingsley, P. and Hume, C.B., 1941, The ore deposits of Nickel Plate Mountain, Hedley, British Columbia: Canadian Inst. of Mining and Metallurgy, Bull., V. XLIV, p. 524-590.

Bostock, H. S., 1930, Geology and ore deposits of Nickel Plate Mountain, Hedley, B. C.: Geol. Surv. Canada, Sum. Rep. 1929, Part A.

_____ 1940a, Map of the Hedley area: Geol. Surv. Canada, Map 568A.

_____ 1940b, Map of the Wolfe Creek area: Geol. Surv. Canada, Map 569A.

Burnham, C.W., and Ohmoto, H., 1980, Late-stage processes of felsic magmatism, *in* Ishihara, S. and Takenouchi, eds., Granitic magmatism and related mineralization: Tokyo, Soc. Mining Geol. Japan, Mining Geol. Spec. Is., No. 8, p. 1-11.

Cameron, D.E., and Garmoe, W.J., 1987, Geology of skarn and high-grade gold in the Carr Fork mine, Utah: Econ. Geol., v. 82, p. 1319-1333.

Camsell, C., 1910, Geology and ore deposits of Hedley mining district, British Columbia: Geol. Survey of Canada, Memoir 2.

Dick, L.A., and Hodgson, C.J., 1982, The Mactung W-Cu(Zn) contact metasomatic and related deposits of the northeastern Canadian Cordillera: Econ. Geol., v. 77, p. 845-867.

Dolmage, V. and Brown, C.E., 1945, Contact metamorphism at Nickel Plate Mountain, Hedley, British Columbia: Canadian Inst. of Mining and Metallurgy, Bull. v. XLVIII, pages 27-68.

Edwards, A. B., and Baker, G., 1954, Scapolitization in the Cloncurry district of north-western Queensland: Jour. Geol. Soc. Australia, v. 1, p 1-33.

Einaudi, M. T., 1982, General features and origin of skarns associated with porphyry copper plutons, southwestern North America, in Titley, S. R., ed., Advances in geology of the porphyry copper deposits, southwestern U. S.: Tucson, Univ. Arizona Press, p. 185-209.

Einaudi, M.T., Meinert, L.D. and Newberry, R.J., 1981, Skarn deposits: Econ. Geol. 75th Anniv. Vol., p. 317-391.

Ettlinger, A. D., and Ray, G. E., 1988, Gold-enriched skarn deposits of British Columbia: B. C. Ministry of Energy, Mines and Petroleum Resources, Geological Fieldwork 1987, Prof. Paper 1988-1, p. 263-279.

_____ 1989, Precious metal enriched skarns in British Columbia - An overview and geologic study: B. C. Ministry of Energy, Mines and Petroleum Resources, Prof. Paper 1989-3, *in press.*

Jacobs, D. C. and Parry, W. T, 1979, Geochemistry of biotite in the Santa Rita prophyry copper deposit, New Mexico: Econ. Geol., v. 74, p. 860-887.

Kuyper, B.A., 1988, Geology of the McCoy gold deposit, Lander County, Nevada, *in* Schafer, R.W., Cooper, J.J. and Vikre, P.G., eds., Bulk mineable precious metal deposits of the western United States: Reno, Geol. Soc. of Nevada, p. 173-186.

Kwak, T. A. P., 1986, Fluid inclusions in skarns (carbonate replacement deposits): Jour. Metamorphic Geol., v. 4, p. 363-384.

Lee, J. W., 1951, The geology of Nickel Plate Mountain, B. C.: Unpub. Ph. D. thesis, Stanford Univ.

Link, J. E., 1985, Gold and copper mineralization in the McCoy Creek district, Skamania County, Washington: Unpub. M.S. thesis, Washington State Univ., 176 p.

Lynch, J. V. G., 1985, Mineralization and alteration zonation of the Kalzas wolframite vein deposit, Yukon Territory, Canada: Unpub. M.S. thesis, Washington State Univ., 123 p.

Meinert, L. D., 1987, Skarn zonation and fluid evolution in the Groundhog mine, Central Mining district, New Mexico: Econ. Geol., v. 82, p. 523-545.

Meinert, L. D., 1984, Mineralogy and petrology of iron skarns in western British Columbia, Canada: Econ. Geol., v. 79, p. 869-882.

Mortimer, N., 1986, Late Triassic, arc-related, potassic igneous rocks in the North American Cordillera: Geology, v. 14, p. 1035-1038.

Newberry, R. J., and Swanson, S. E., 1986, Scheelite skarn granitoids: An evaluation of the roles of magmatic source and process: Ore Geol. Rev., v. 1, p. 57-81.

Potter, R.W., II, Babcock and Brown, D. L, 1977, A new method for determining the solubility of salts in aqueous solutions at elevated temperatures: Jour. Research U.S. Geol. Surv., v. 5 (3), p. 389-395.

Preto, V.A., 1972, Geology of Copper Mountain: B.C. Ministry of Energry, Mines and Petroleum Resources, Bull. 59.

_____ 1977, The Nicola Group: Mesozoic volcanism related to rifting in southern British Columbia, *in*, Volcanic Regimes in Canada: W. R. A. Baragar, L. C. Coleman and J. M. Hall, eds., Geological Association of Canada, Spec. Paper 16, p. 39-57.

Ray, G.E. and Dawson, G.L. 1987, Geology and mineral occurrences in the Hedley Gold Camp: B.C. Ministry of Energy, Mines and Petroleum Resources, O. F. Maps 1987-10a, 10b, 10c.

Ray, G.E., Dawson, G.L. and Simpson, R., 1987, The geology and controls of skarn mineralization in the Hedley gold camp, Southern British Columbia: B.C. Min. of Energy, Mines and Petrol. Resources, Geol. Fieldwork, 1986, P. 1987-1, p. 65-79.

_____ 1988, The geology, geochemistry and metallogenic zoning in the Hedley gold-skarn camp: B.C. Min. of Energy, Mines and Petrol. Resources, Geol. Fieldwork, 1987, Paper 1988-1, p. 59-80.

Rice, H.M.A., 1947, Geology and mineral dDeposits of the Princeton map-area, with Maps 888A and 889A: Geol. Survey of Canada Memoir 243.

Roedder, E., 1984, Fluid inclusions: Rev. in Mineralogy, v. 12, 644 p.

Simpson, R. and Ray, G.E., 1986, Nickel Plate gold mine: Canadian Inst. of Mining and Metallurgy, Dist. 6 Meeting, P. No. 30, 8 p.

Shepherd, T. J., Rankin, A. H., and Alderton, D. H. M., 1985, A practical guide to fluid inclusion studies: Blackie & Son Ltd., London, 239 p.

Streckeisen, A. and Lemaitre, R.W.L., 1979, A chemical approximation to the modal QAPF classification of the igneous rocks: N. Jb. Miner. Abh., v. 136, p. 169-206.

Sterner, S. M., Hall, D. L., and Bodnar, R. J., 1988, Synthetic fluid inclusions. Solubility relations in the system NaCl-KCl-H20 under vapor saturated conditions: Geochem. Cosmochem. Acta, v. 52, p. 989-1005.

Titley, S. R., and Beane, R. E., 1981, Porphyry copper deposits-Part 1. Geologic settings, petrology, and tectogenesis: Econ. Geol., 75th Anniv. Vol., p. 214-235.

Torrey, C. E., 1986, Geology and genesis of the Red Dome (Mungana) gold skarn deposit, North Queensland: Unpub. M. Sc. thesis, James Cook University, 359 p.

Warren, H. V., and Cummings, J. M., 1936, Mineralogy at the Nickel Plate mine: Miner, v. 9, p. 27-28.

Wheeler, J.O., Brookfield, A.J., Gabrielse, H., Monger, J.W.H., Tipper, H.W., and Woodsworth, G.J., 1988, PReliminary terrane map of the Canadian Cordillera, (1:2 000 000), in Decade of North American Geology, *in preparation.*

Wotruba, P.R., Benson, R.G. and Schmidt, K.W. (1986): Battle Mountain Describes the Geology of its Fortitude Gold-Silver Deposit at Copper Canyon, Mining Enginering, vol. 38, 495-499.

Tables

Table 1. Representative electron microprobe analyses of biotite, amphibole and plagioclase alteration products in endoskarn.

Table 2. Representative electron microprobe analyses of pyroxene from the Nickel Plate deposit.

Table 3. Representative electron microprobe analyses of garnet and wollastonite from the Nickel Plate deposit.

Table 4. Representative electron microprobe analyses of sulfide minerals from the Nickel Plate deposit.

Table 5. Correlation between endoskarn and exoskarn alteration stages in the Nickel Plate deposit.

Figures

Fig. 1. Location and surface geology of the Hedley district (compiled from Monger and Price, 1979; Ray et al., 1988; and Gabrielse and Yorath, 1989).

Fig. 2. Geochemistry of the Hedley intrusions compared to porphyry-Cu and other related plutons. A. Alkali-silica plot illustrating the island-arc affinity of the Hedley intrusions. B. Alkali-CaO ternary diagram further showing the similarities between Pacific and Caribbean island-arc plutons and the Hedley intrusions. C. Orthoclase-quartz-plagioclase normative ternary illustrating the orthoclase-quartz deficiency of the Hedley intrusions relative to porphyry-Cu plutons. The Hedley intrusions are most similar to intrusions associated with Fe-Au skarns in Alaska. D. Normative classification of plutonic rocks after Streckeisen and Le Maitre (1979) showing the quartz diorite nature of the Hedley intrusions and their distinction from W-skarn granitoids. Hedley data from Ray et al., 1988, other data adapted from Titley and Beane, 1981; and Newberry and Swanson, 1986.

Fig. 3. Surface geology of Nickel Plate Mt (Mascot Gold Mines Ltd. staff geologists). Line of section A-B-C (Fig. 4) and approximate location of current open pit is also shown.

Fig. 4. Cross section through the Nickel Plate deposit (*see* Fig. 3 for location).

Fig. 5. Photomicrographs of alteration styles in Hedley intrusion diorite. A. Remnant diorite from core of thick sill. B. Early Mg-rich pyroxene replacing igneous amphibole. C. Pyroxene-K-spar-pyrrhotite veinlets cutting diorite. D. Massive pyroxene-garnet skarn replacement of diorite. Note complete destruction of igneous texture.

Fig. 6. Comparison of hydrothermal biotite in the Nickel Plate deposit with biotite from the Santa Rita (Jacobs and Parry, 1979) and McCoy Creek (Link, 1985) porphyry copper deposits and the Kalzas wolframite vein deposit (Lynch, 1985).

Fig. 7. Composition of endoskarn pyroxene formed in the Hedley intrusions. See text for discussion.

Fig. 8. Composition of garnet (A) and pyroxene (B) from the Nickel Plate deposit.

Fig. 9. Distribution of skarn minerals and sulfide-Au mineralization in the Nickel Plate deposit.

Fig. 10. Variation in garnet and pyroxene abundance across the deposit.

Fig. 11. Compositional variation in garnet (mole % Ad) and pyroxene (mole % Hd and Jo) across the Nickel Plate deposit.

Fig. 12. Sketch illustrating spatial relationships between endoskarn and exoskarn alteration styles in the Nickel Plate deposit.

Fig. 13. Fluid inclusion homogenization temperatures of garnet (A), pyroxene (B) and quartz and scapolite (C) from the Nickel Plate deposit.

Fig. 14. Plot of mole fraction Hd versus mole fraction Ad illustrating the similarities in the reduced nature of calc-silicate skarn from W-skarns and the Nickel Plate deposit relative to porphyry-Cu skarns (porphyry-Cu and W-skarn data from Einaudi, 1982 and quoted sources).

Fig. 15. Hedenbergite versus johansennite composition of exoskarn pyroxene from the Nickel Plate deposit. Two populations of pyroxene are represented by the compositional trend found in the ore zone, and from the divergence from this trend of pyroxene nearer the Toronto stock.

Fig. 16. Andradite versus pyralspite composition of garnet from the Nickel Plate deposit. As in pyroxene (*see* Fig. 15), two populations of garnet are also suggested.

Fig. 17. Contoured cross section of average fluid inclusion homogenization temperatures for garnet (A) and pyroxene (B). See text for discussion.

Fig. 18. Variation in pyroxene fluid inclusion homogenization temperature with depth in two drill holes from the Nickel Plate deposit.

Fig. 19. Log fO_2-Log fS_2 diagram showing stability fields of major calc-silicate and sulfide minerals at 500°C and XCO_2=0.1. Stability field of hedenbergitic skarn at Nickel Plate shown as shaded area. Mineral stabilities from Meinert (1980).

Fig. 20. A. Variation in Fe and S-content of pyrrhotite across the Nickel Plate deposit. B. Composition of pyrrhotite in atom percent Fe as a function of T-log fS_2 from Barton and Skinner (1979). Heavy line with arrow shows a cooling path from higher temperature, low-Fe pyrrhotite found near the Toronto stock (point A), and lower temperature, higher-Fe pyrrhotite from near the marble line (point B).

Fig. 21. Variation in As content of arsenopyrite as a function of T-log fS_2 from Kretschmar and Scott (1976). Shaded area shows range of arsenopyrite compositions from the Nickel Plate deposit.

Fig. 22. Log fO2-Log fS2 diagram at T=300°C showing stability fields of major sulfide minerals found in the Nickel Plate deposit. Shaded area shows stability field of Au-sulfide assemblage from the deposit. Mineral stability fields from Barton and Skinner (1979) and quoted sources therein.

Fig. 23. Diagram summarizing temperature, mineralogical and geochemical patterns observed in the Nickel Plate deposit. Also shown are possible hydrothermal fluid paths which are suggested by the indicated patterns. See text for detailed discussion.

Table 1. Representative electron microprobe analyses of biotite, amphibole and plagioclase alteration products in endoskarn.

Mineral	Biotite	Biotite	Amph.	Amph.	Plag.	Plag.
Description	1	1	2	3	4	5
Sample #	195.25.0	195.25.0	195.25.0	195.25.0	195.25.0	195.25.0
NaO	0.12	0.05	2.00	0.26	3.55	8.35
FeO*	18.00	21.55	13.80	11.19	0.51	0.08
K2O	9.29	9.61	0.43	0.12	0.08	0.24
SiO2	33.35	35.67	45.98	54.47	50.94	60.69
CaO	0.10	0.01	11.97	12.73	13.85	5.43
Al2O3	20.42	18.88	9.57	1.78	30.49	24.03
TiO2	0.50	1.75	1.00	0.04	0.05	0.00
MgO	12.36	7.66	12.57	16.30	0.06	0.01
MnO	0.11	0.80	0.25	0.11	0.05	0.02
OH	3.91	3.92	-	-	-	-
Total	98.16	99.89	97.56	96.99	99.57	98.84

*All iron as FeO
- not determined

Number of Ions						
Na	0.03	0.02	0.57	0.07	0.31	0.73
Fe	2.31	2.76	1.70	1.35	0.02	0.00
K	1.82	1.88	0.08	0.02	0.00	0.01
Si	5.12	5.46	6.78	7.84	2.33	2.73
Ca	0.02	0.21	1.89	1.96	0.68	0.26
Al	3.70	3.41	1.66	0.30	1.65	1.27
Ti	0.06	0.20	0.11	0.00	0.00	0.00
Mg	2.83	1.75	2.76	3.50	0.00	0.06
Mn	0.01	0.10	0.03	0.01	0.00	0.06
OH	4.00	4.00	-	-	-	-
	19.90	19.58	15.58	15.06	5.00	5.01
				Ab	31.5	72.6
				Or	0.5	1.4
				An	68.0	26.0

Descriptions:
1 - Replaces amphibole
2 - Remnant igneous amphibole
3 - Secondary amphibole
4 - Primary phenocryst
5 - Secondary plagioclase on sill margin

Table 2. Representative electron microprobe analyses of pyroxene from the Nickel Plate deposit.

Descriptio	Distal	Distal	Mn-rich	Mn-rich	Mn-rich	Mn-rich	Massive	Massive
Protolith	Limestone	Limestone	Siltstone	Siltstone	Limestone	Siltstone	Siltstone	Siltstone
Sample #	262.127.7	262.127.7	514.360	514.360	135.141.7	262.96.2	195.20.7	262.38.5
Na2O	0.43	0.29	0.15	0.07	0.02	0.05	0.09	0.11
FeO*	0.00	0.28	11.39	11.47	23.75	23.01	21.47	21.03
K2O	0.00	0.00	0.03	0.00	0.04	0.01	0.02	0.00
SiO2	55.11	54.74	52.08	52.23	49.59	50.11	50.23	49.32
CaO	25.42	25.59	24.60	24.76	23.36	23.26	23.52	23.87
Al2O3	1.59	0.73	0.18	0.15	0.07	0.07	0.10	0.23
TiO2	0.06	0.02	0.02	0.01	0.00	0.01	0.00	0.03
MgO	17.17	17.54	9.90	9.68	2.12	2.54	3.68	4.22
MnO	0.09	0.09	2.25	2.41	1.10	1.68	0.81	0.90
TOTAL	99.87	99.28	100.60	100.78	100.05	100.74	99.92	99.71

All iron as FeO

Na	0.030	0.020	0.011	0.005	0.002	0.004	0.007	0.009
Fe	0.000	0.009	0.364	0.366	0.803	0.771	0.718	0.706
K	0.000	0.000	0.001	0.000	0.002	0.001	0.001	0.000
Si	1.987	1.991	1.988	1.991	2.006	2.007	2.008	1.981
Ca	0.982	0.997	1.006	1.011	1.012	0.998	1.008	1.027
Al	0.068	0.031	0.008	0.007	0.003	0.003	0.005	0.011
Ti	0.002	0.001	0.001	0.000	0.000	0.000	0.000	0.001
Mg	0.922	0.951	0.563	0.550	0.128	0.152	0.219	0.253
MN	0.003	0.003	0.073	0.078	0.038	0.057	0.027	0.031
Sum	3.99	4.00	4.01	4.01	3.99	3.99	3.99	4.02

Cations based on 6 oxygens

mole %								
Jo	0.3	0.3	7.3	7.8	3.9	5.8	2.8	3.1
Di	99.7	98.8	56.3	55.4	13.2	15.5	22.7	25.5
Hd	0.0	0.9	36.4	36.8	82.9	78.7	74.4	71.4

Table 2.

Descriptio	Hornfels	Hornfels	Early	Early	Vein	Vein	Massive	Massive
Protolith	Siltstone	Siltstone	Diorite	Diorite	Diorite	Diorite	Diorite	Diorite
Sample #	378.77A	378.77A	378.67.4	195.25.2	378.102B	378.102B	378.116.9	378.116.9
Na2O	0.05	0.07	0.19	0.21	0.12	0.11	0.10	0.11
FeO*	16.19	14.59	5.63	4.61	12.82	11.96	15.90	17.44
K2O	0.00	0.00	0.00	0.03	0.00	0.00	0.00	0.02
SiO2	51.50	52.01	53.68	53.20	52.19	52.69	51.59	51.06
CaO	24.12	24.37	24.77	24.90	23.87	24.32	23.80	23.67
Al2O3	0.08	0.40	0.42	0.57	0.28	0.33	0.16	0.22
TiO2	0.02	0.00	0.06	0.03	0.03	0.04	0.01	0.04
MgO	7.53	8.49	14.35	14.96	9.56	10.16	7.53	6.83
MnO	0.72	0.88	0.18	0.15	0.88	0.90	0.52	0.53
TOTAL	100.21	100.81	99.28	98.66	99.75	100.50	99.62	99.91

*All iron

Na	0.004	0.005	0.014	0.015	0.009	0.008	0.008	0.008
*Fe	0.526	0.468	0.175	0.144	0.412	0.380	0.518	0.571
K	0.000	0.000	0.000	0.001	0.000	0.000	0.000	0.001
Si	2.001	1.994	1.998	1.987	2.003	2.000	2.010	1.999
Ca	1.004	1.001	0.988	0.997	0.982	0.989	0.993	0.993
Al	0.004	0.018	0.018	0.025	0.013	0.015	0.007	0.010
Ti	0.001	0.000	0.002	0.001	0.001	0.001	0.000	0.001
Mg	0.436	0.485	0.796	0.833	0.547	0.575	0.437	0.398
MN	0.024	0.029	0.006	0.005	0.029	0.029	0.017	0.018
Sum	4.00	4.00	4.00	4.01	3.99	4.00	3.99	4.00

Cations ba

mole %								
Jo	2.4	2.9	0.6	0.5	2.9	2.9	1.8	1.8
Di	44.2	49.4	81.5	84.8	55.4	58.4	45.0	40.4
Hd	53.4	47.7	17.9	14.7	41.7	38.6	53.3	57.8

Table 3. Representative electron microprobe analyses of garnet and wollastonite from the Nickel Plate deposit.

Mineral	Garnet	Garnet	Garnet	Garnet	Garnet	Garnet	Woll.	Woll.
Descriptio	Core	Rim	Vein-Euhed	Core	Overgrowth	Poikolitic		
Protolith	Siltstone	Siltstone	Diorite	Siltstone	Siltstone	Siltstone	Siltstone	Siltstone
Sample #	514.86	514.86	514.181B	378.78.5	378.78.5	262.38.5	378.71.9A	378.71.9A
Na2O	0.00	0.01	0.02	0.07	0.00	0.00	0.03	0.02
Fe2O3*	5.37	6.20	8.42	26.04	20.06	9.78	2.84	5.09
K2O	0.00	0.00	0.01	0.01	0.00	0.00	0.04	0.00
SiO2	39.52	39.24	38.21	36.72	37.68	37.51	50.71	50.39
CaO	36.03	36.34	34.87	34.24	34.64	34.63	44.67	42.24
Al2O3	19.32	18.83	16.46	3.67	8.40	16.58	0.04	2.59
TiO2	0.00	0.07	1.28	0.12	0.24	0.37	0.00	0.11
MgO	0.00	0.04	0.06	0.08	0.05	0.03	0.49	0.00
MnO	0.69	0.82	0.79	0.15	0.28	0.58	0.32	0.26
TOTAL	100.93	101.55	100.12	101.10	101.35	99.48	99.14	100.70

*FeO in wollastonite

Na	0.003	0.000	0.003	0.011	0.000	0.000	0.001	0.001
Fe	0.350	0.508	0.490	1.605	1.202	0.575	0.047	0.082
K	0.001	0.001	0.001	0.001	0.000	0.000	0.001	0.000
Si	2.981	2.988	2.956	3.008	3.001	2.931	0.996	0.974
Ca	2.930	2.898	2.891	3.005	2.957	2.899	0.940	0.874
Al	1.668	1.515	1.501	0.354	0.789	1.527	0.001	0.059
Ti	0.023	0.025	0.074	0.007	0.014	0.022	0.000	0.002
Mg	0.002	0.009	0.007	0.010	0.006	0.003	0.014	0.000
MN	0.032	0.032	0.052	0.010	0.019	0.038	0.005	0.004
Sum	7.99	7.98	7.98	8.01	7.99	8.00	2.00	2.00

Cations bad on 12 Oxygens:

Mole %						
Pyral	1.1	1.4	2.0	0.7	0.8	1.3
Gross	81.5	73.5	73.4	17.4	38.8	71.3
And	17.3	25.1	24.6	81.9	60.4	27.4

Table 4. Representative electron microprobe analyses of sulfide minerals from the Nickel Plate deposit.

	Gold	Gold	Hedleyite	Arseno.	Arseno.	Arseno.	Sphal.	Sphal.
BI	0.00	0.00	77.95	0.01	0.71	0.15	0.00	0.00
AS	2.59	2.91	3.85	47.53	41.05	47.71	0.02	0.09
S	0.10	0.14	0.01	18.15	22.15	18.08	33.24	33.43
ZN	-	-	-	-	0.05	-	58.25	54.20
AG	10.28	19.29	0.00	0.00	0.00	0.00	0.00	0.00
CD	-	-	-	-	0.00	-	0.88	1.17
AU	88.62	78.01	0.00	0.14	0.00	0.04	0.01	0.00
CO	0.12	0.11	0.12	1.33	0.00	4.15	0.00	0.00
TE	0.00	0.01	19.99	0.00	0.00	0.05	0.03	0.00
FE	1.15	1.21	0.88	33.28	35.79	30.62	7.04	10.41
CU	0.02	0.00	0.00	0.00	-	0.00	-	-
TOTAL	102.89	101.69	102.81	100.44	99.75	100.80	99.47	99.30

- Not analyzed

Table 5. Correlation between endoskarn and exoskarn alteration stages in the Nickel Plate deposit.

	Exoskarn	Endoskarn Equivalent
Early		
T i m e	1)Isochemical recryst. of sediments	None. Sill-dike emplacement
	2)Bioite hornfels	Biotite-amphibole alteration of mafic phenocrysts, k-spar alteration of matrix
	3)Pyroxene and k-spar hornfels	Pyroxene alteration of biotite and early pyroxene-k-spar-pyrrhotite veins
	4)Scapolitization of marble	Na-Ca metasomatism of sill contacts
	5)Pyroxene-garnet skarn	Massive pyroxene-garnet
	6)Wollastonite-calcite-epidote	Epidote-wollastonite-calcite
	7)Scapolite-arsenopyrite-Bi-Te-Au	Scapolite-epidote-clinozoisite
	8)Pyrrhotite-prehnite	Pyrrhotite-arsenopyrite-prehnite
Late		

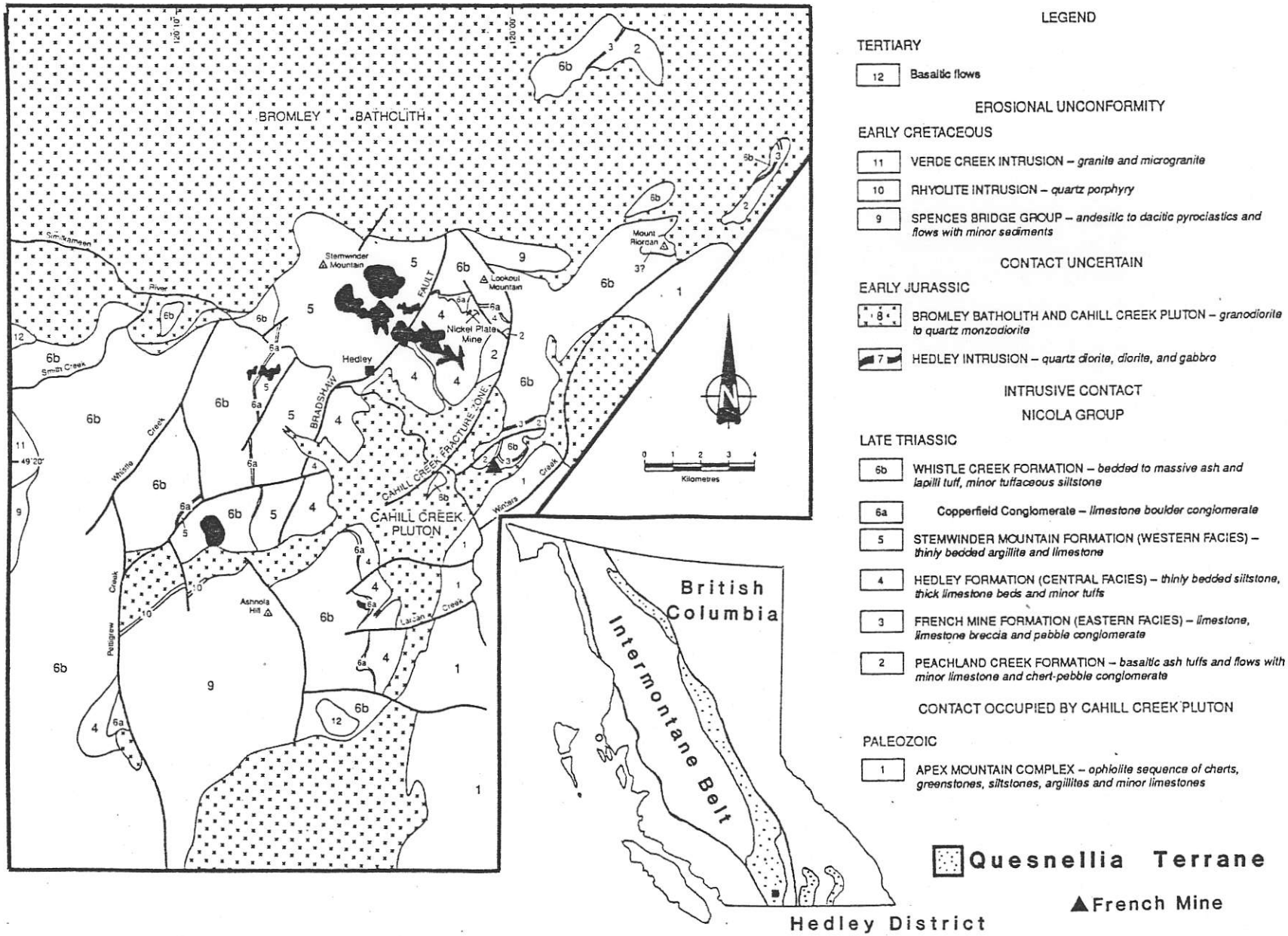

LEGEND

TERTIARY

12 Basaltic flows

EROSIONAL UNCONFORMITY

EARLY CRETACEOUS

11 VERDE CREEK INTRUSION – *granite and microgranite*

10 RHYOLITE INTRUSION – *quartz porphyry*

9 SPENCES BRIDGE GROUP – *andesitic to dacitic pyroclastics and flows with minor sediments*

CONTACT UNCERTAIN

EARLY JURASSIC

8 BROMLEY BATHOLITH AND CAHILL CREEK PLUTON – *granodiorite to quartz monzodiorite*

7 HEDLEY INTRUSION – *quartz diorite, diorite, and gabbro*

INTRUSIVE CONTACT

NICOLA GROUP

LATE TRIASSIC

6b WHISTLE CREEK FORMATION – *bedded to massive ash and lapilli tuff, minor tuffaceous siltstone*

6a Copperfield Conglomerate – *limestone boulder conglomerate*

5 STEMWINDER MOUNTAIN FORMATION (WESTERN FACIES) – *thinly bedded argillite and limestone*

4 HEDLEY FORMATION (CENTRAL FACIES) – *thinly bedded siltstone, thick limestone beds and minor tuffs*

3 FRENCH MINE FORMATION (EASTERN FACIES) – *limestone, limestone breccia and pebble conglomerate*

2 PEACHLAND CREEK FORMATION – *basaltic ash tuffs and flows with minor limestone and chert-pebble conglomerate*

CONTACT OCCUPIED BY CAHILL CREEK PLUTON

PALEOZOIC

1 APEX MOUNTAIN COMPLEX – *ophiolite sequence of cherts, greenstones, siltstones, argillites and minor limestones*

Quesnellia Terrane

▲French Mine

Figure 1

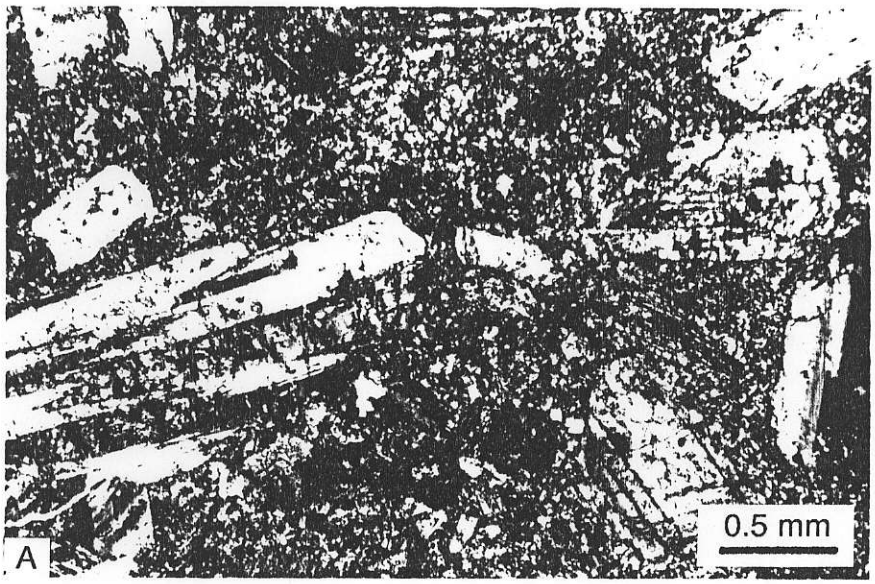

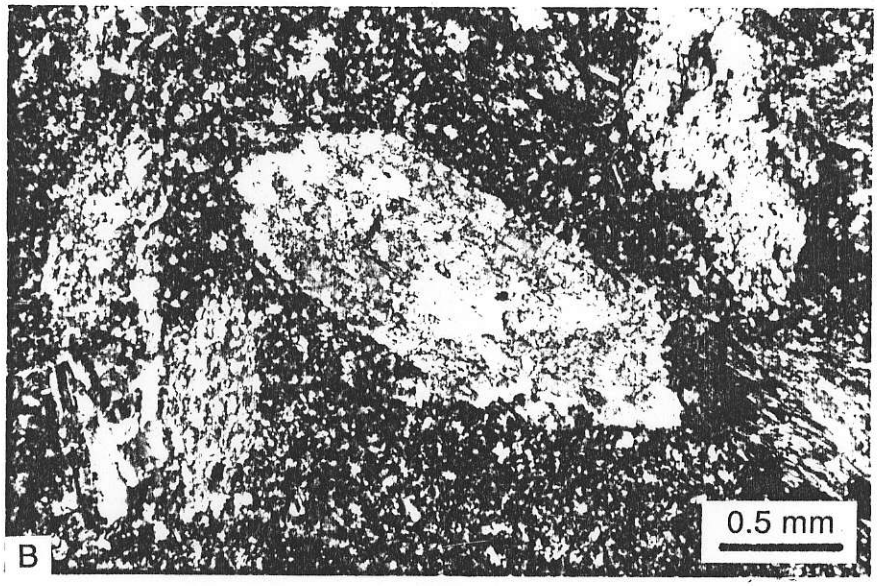

Figure 5

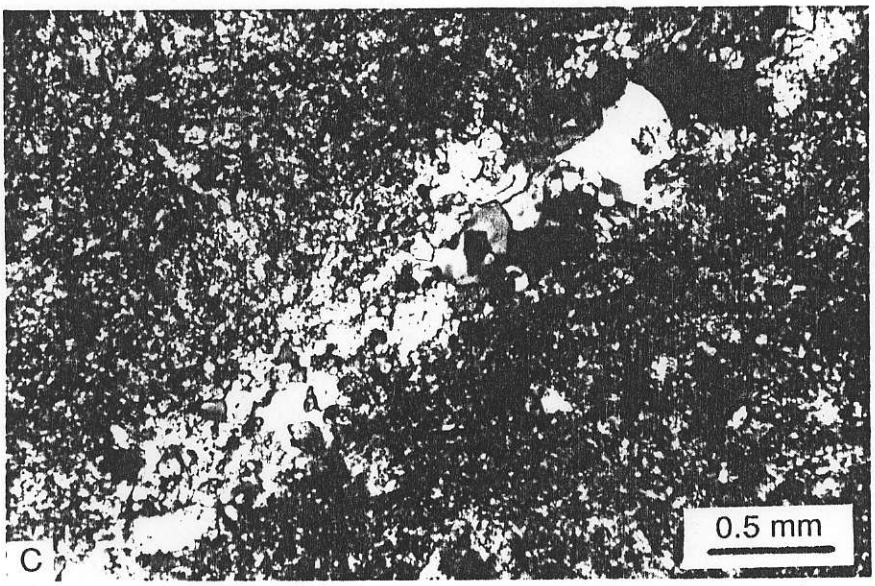

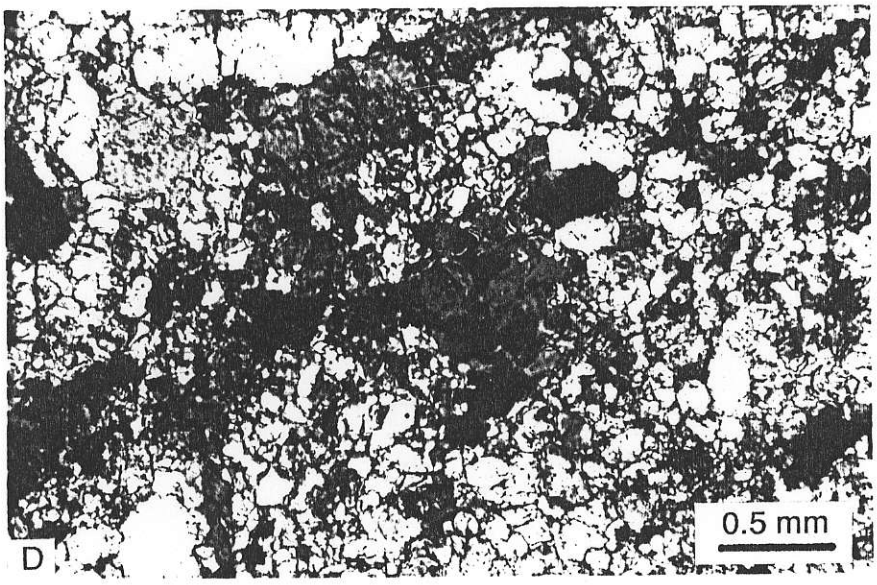

Figure 5

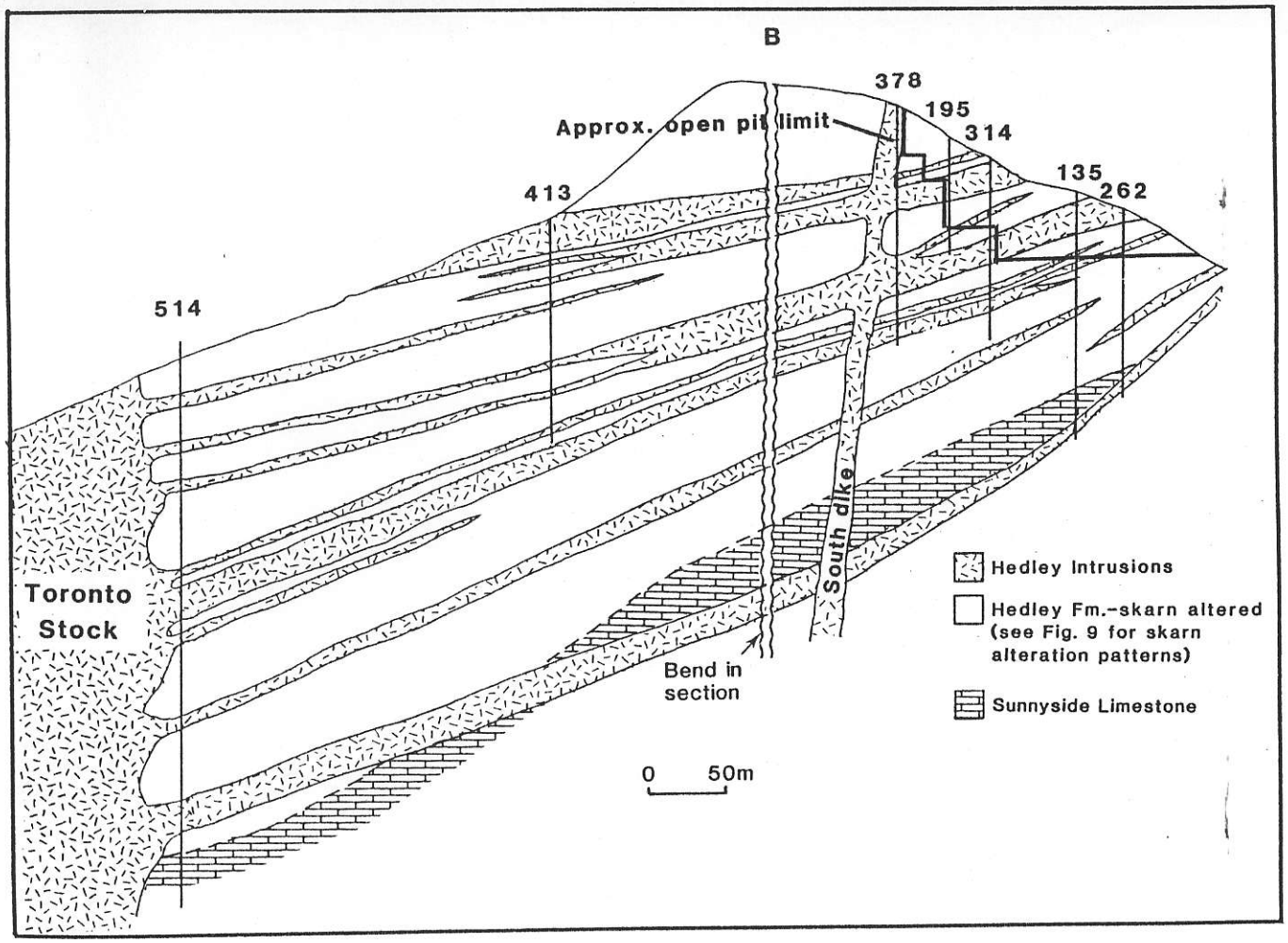

Figure 4

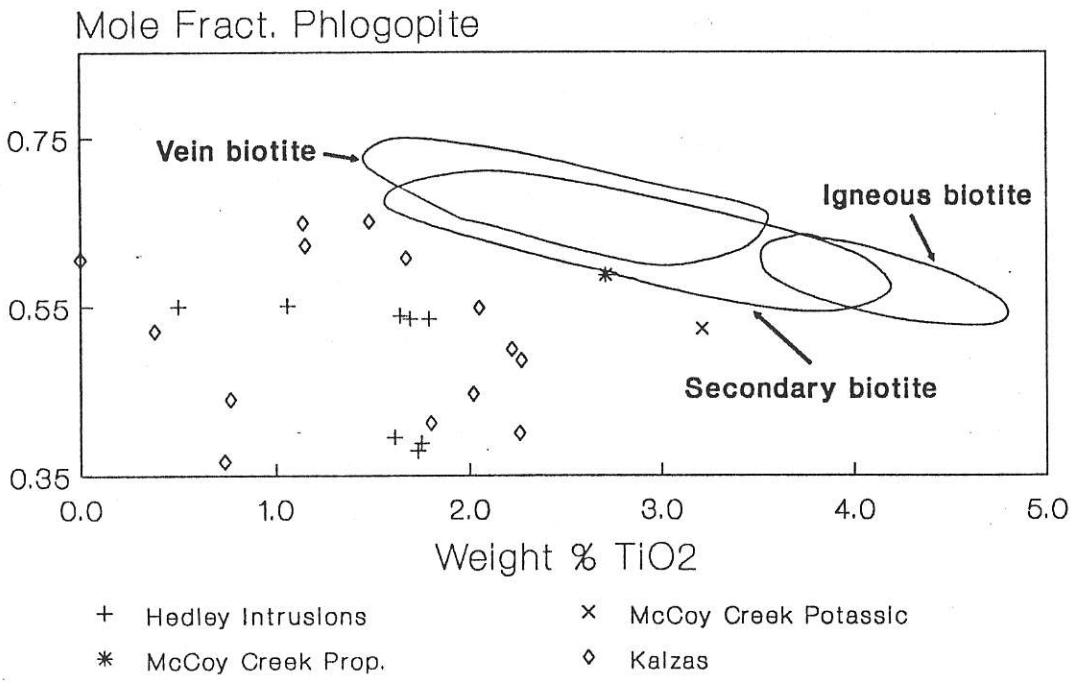

Figure 6

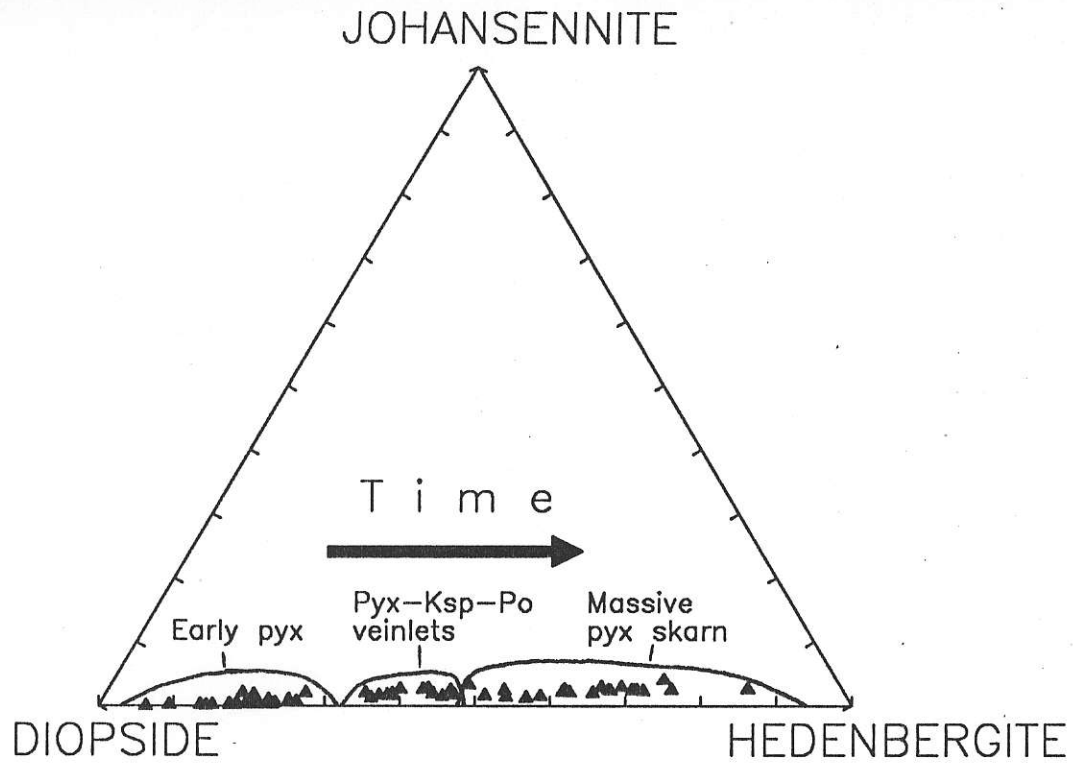

Figure 7

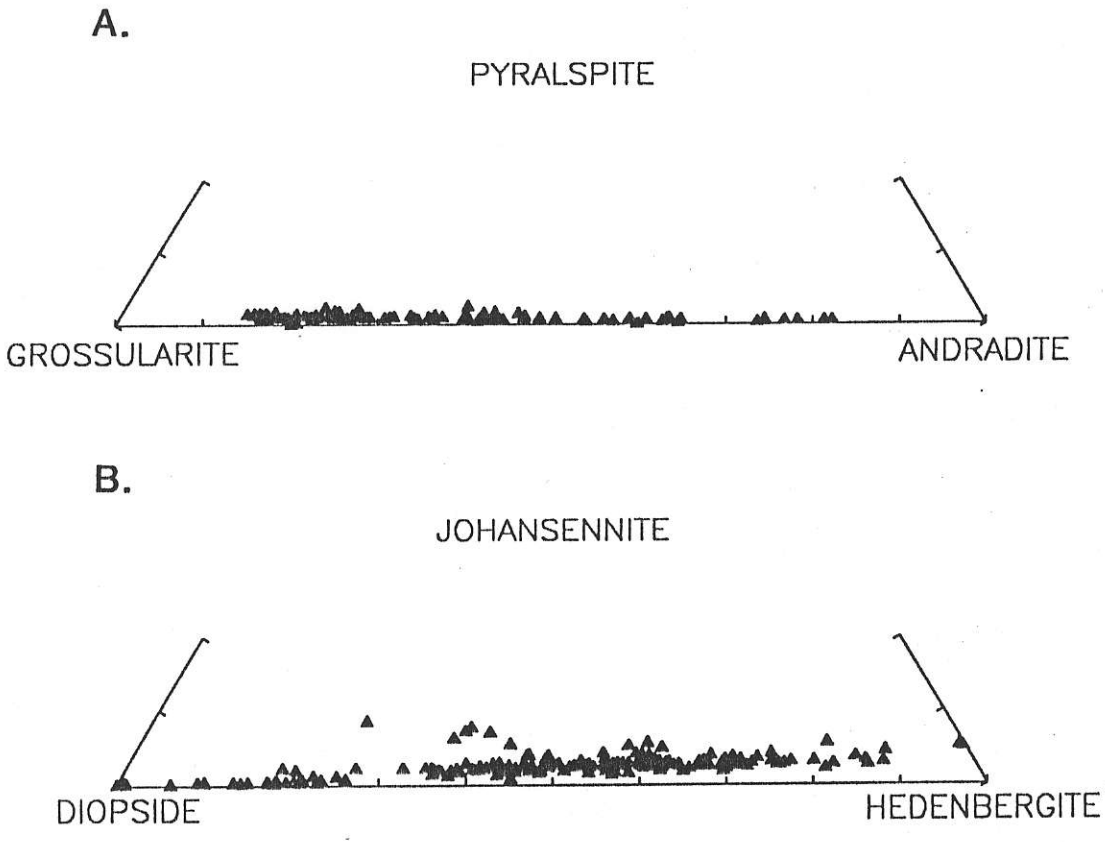

Figure 8

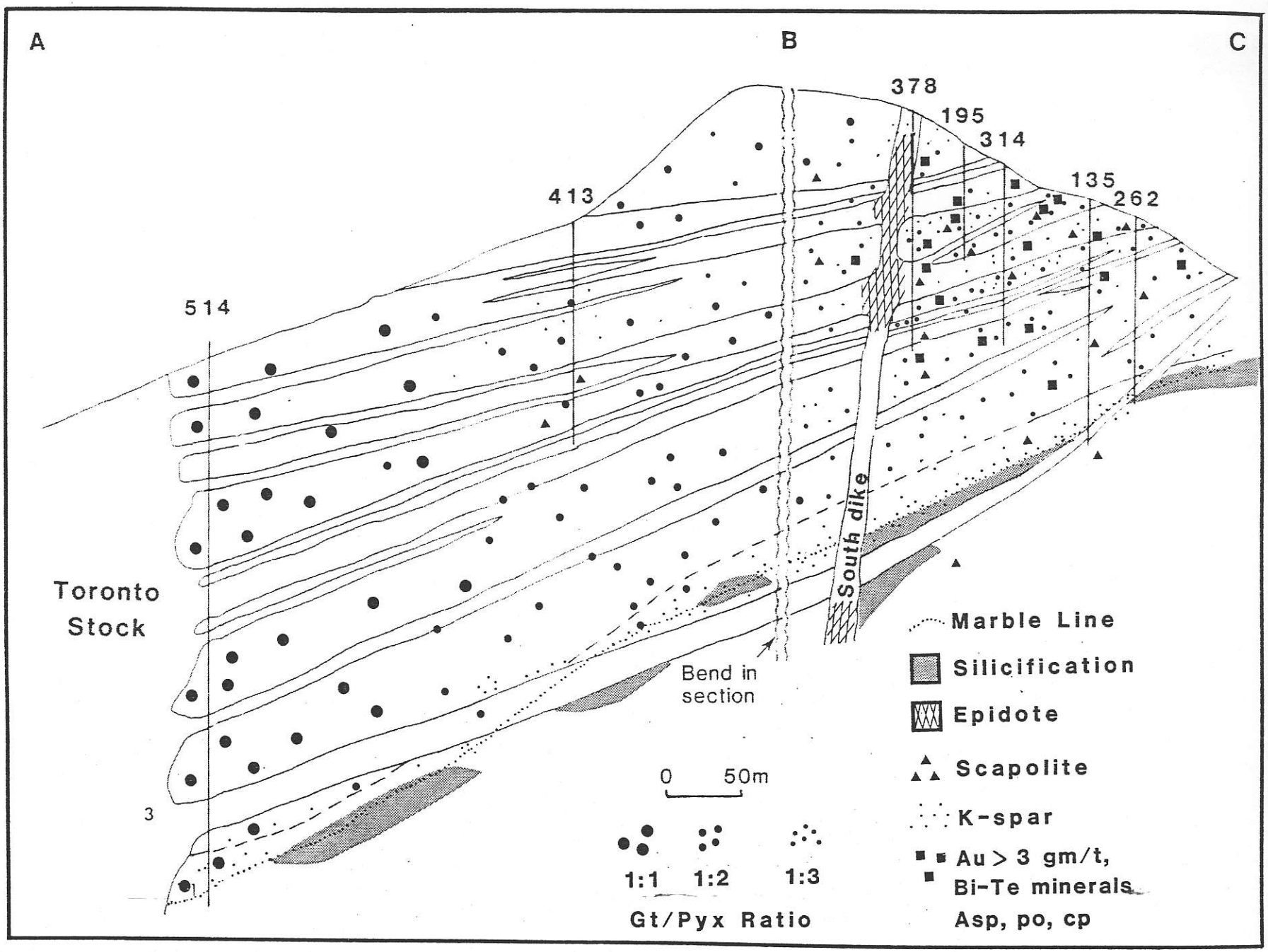
A
B
C
378
195
314
135
262
413
514
South dike
Toronto
Stock
Bend in
section
3
1
0 50m
1:1 1:2 1:3
Gt/Pyx Ratio
Marble Line
Silicification
Epidote
Scapolite
K-spar
Au > 3 gm/t,
Bi-Te minerals
Asp, po, cp

Figure 9

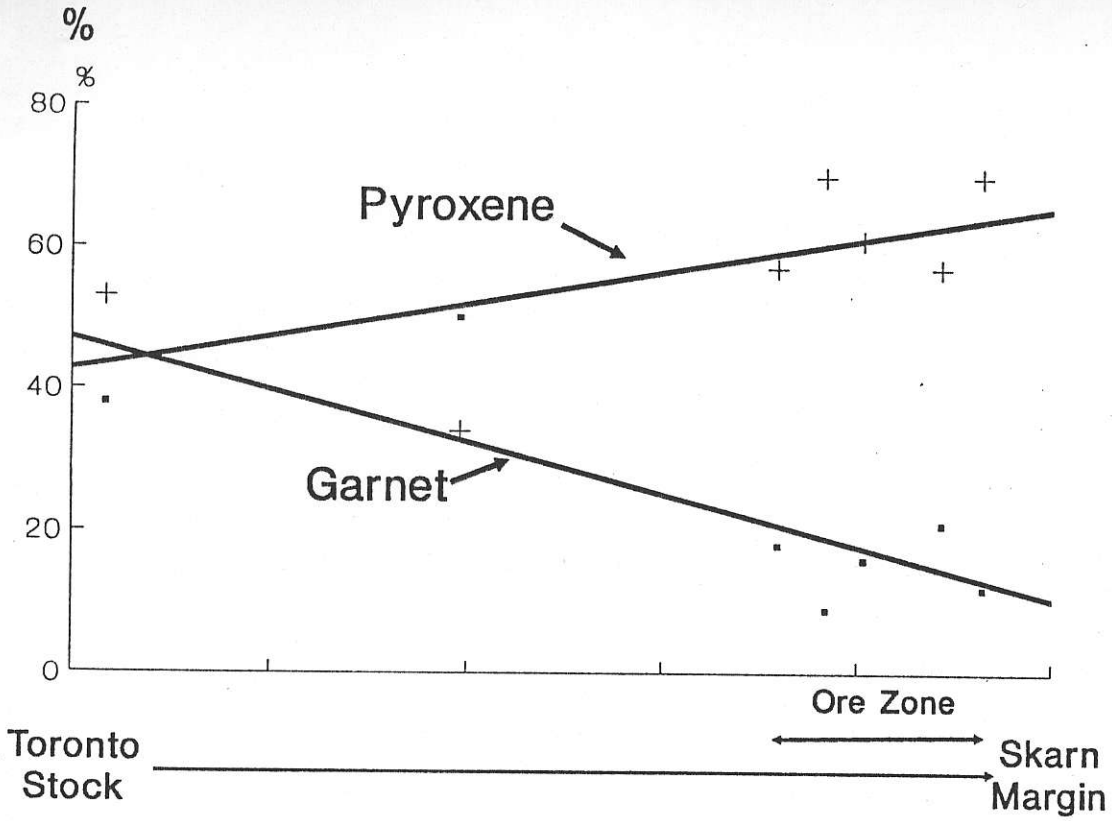

Figure 10

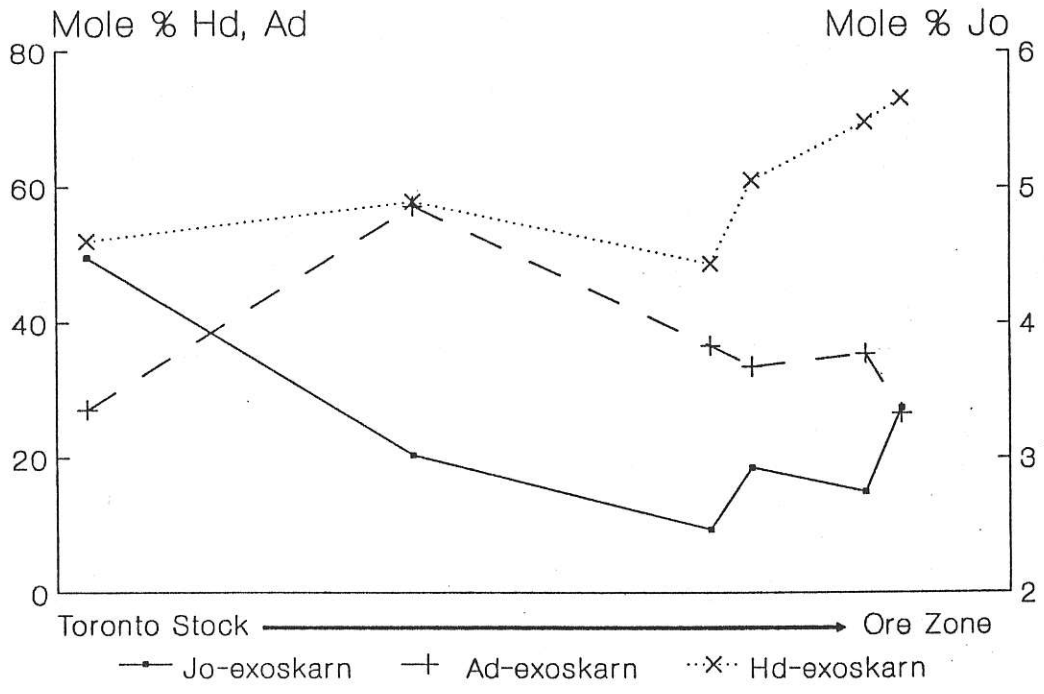

Figure 11

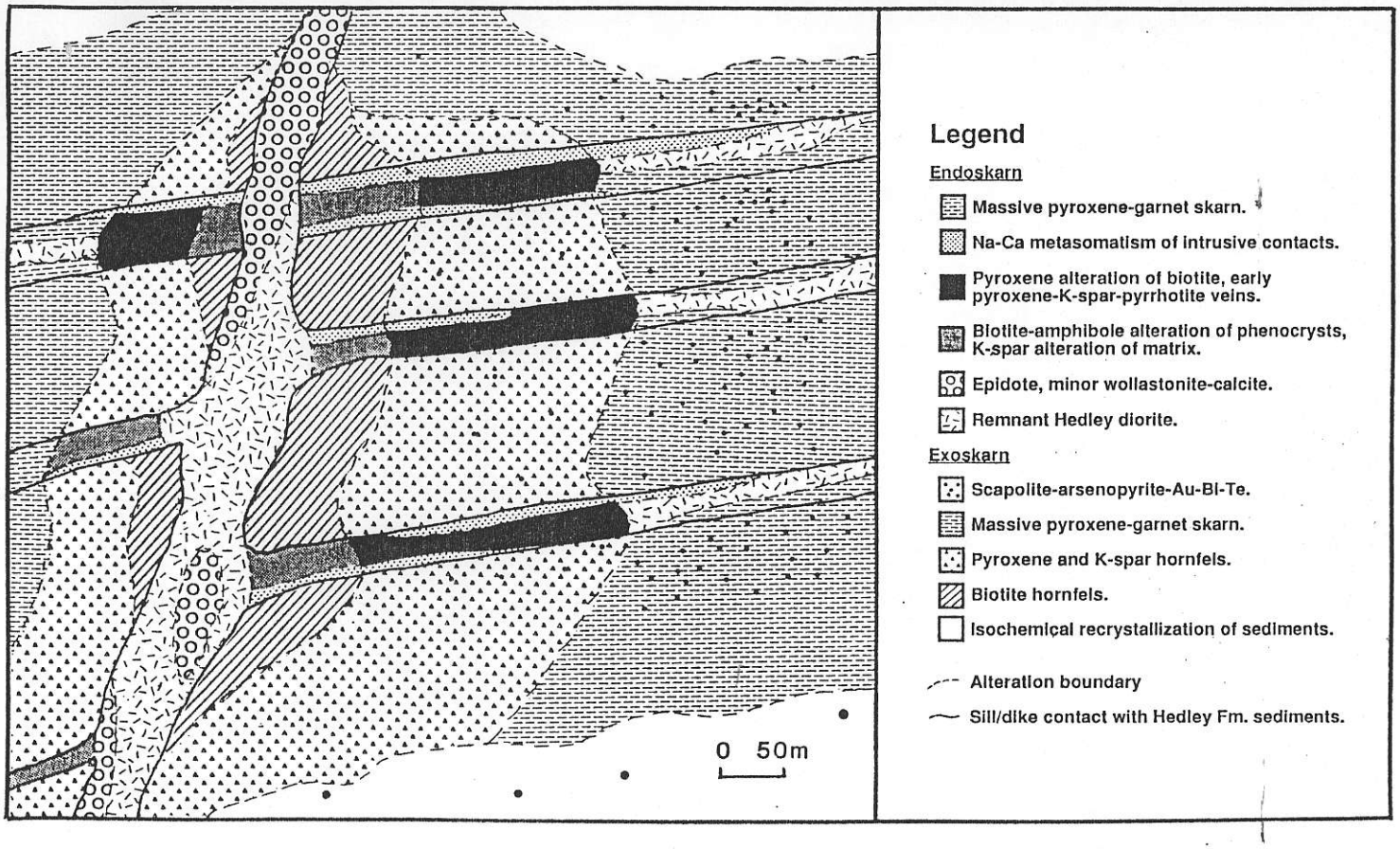

Figure 12

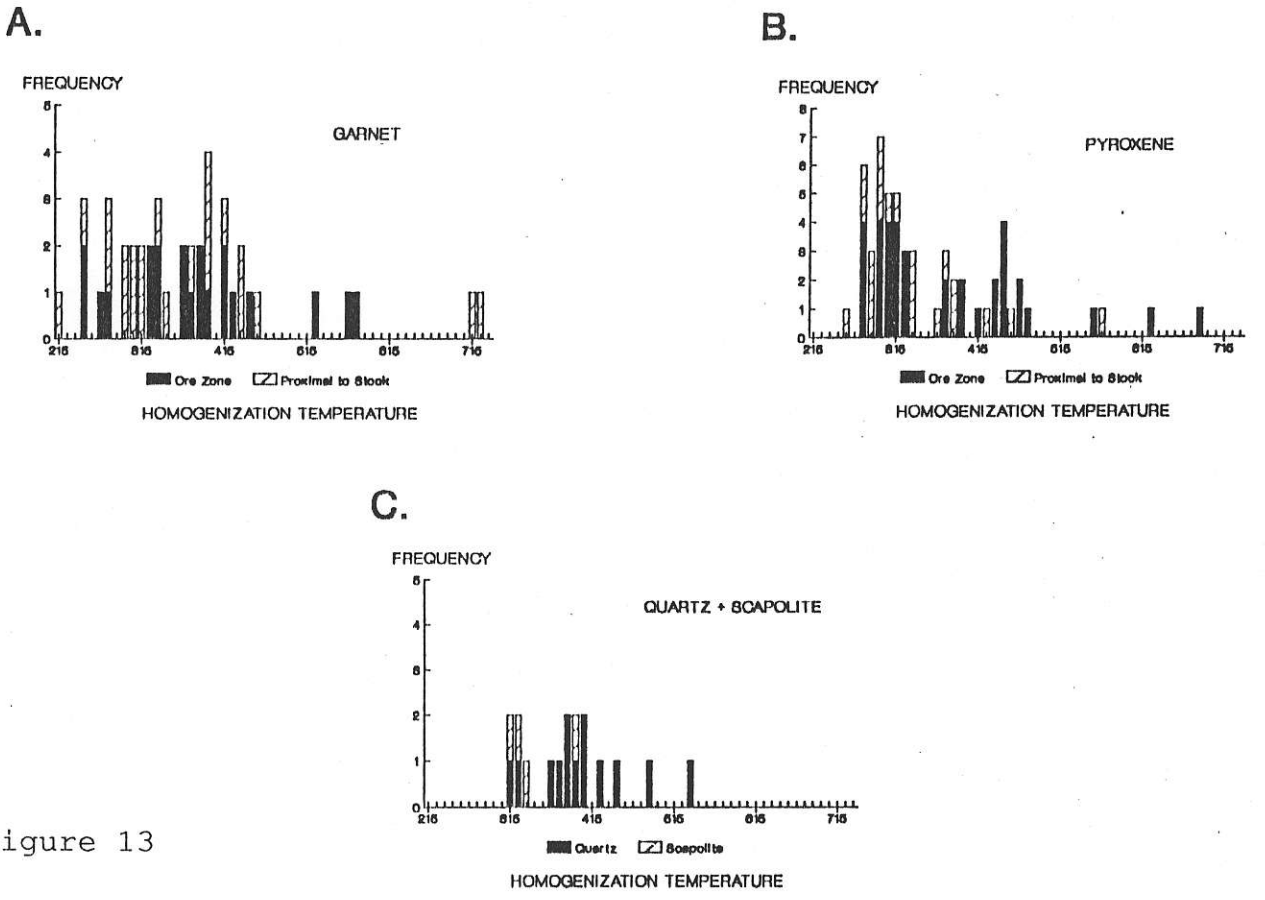

Figure 13

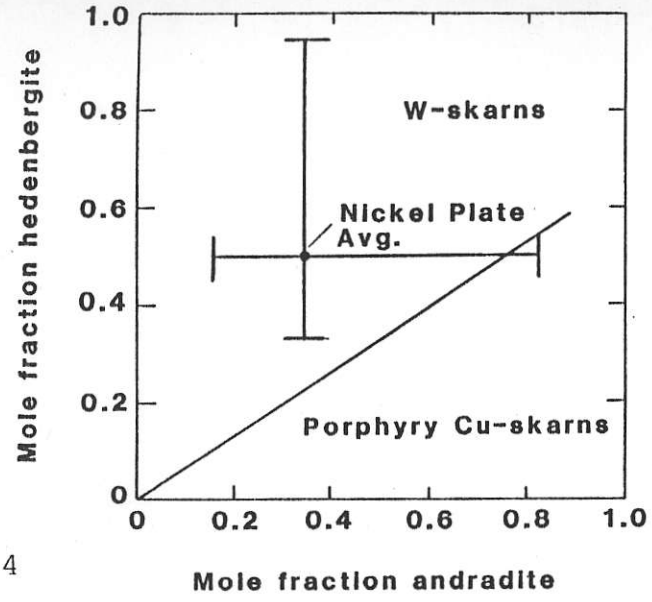

Figure 14

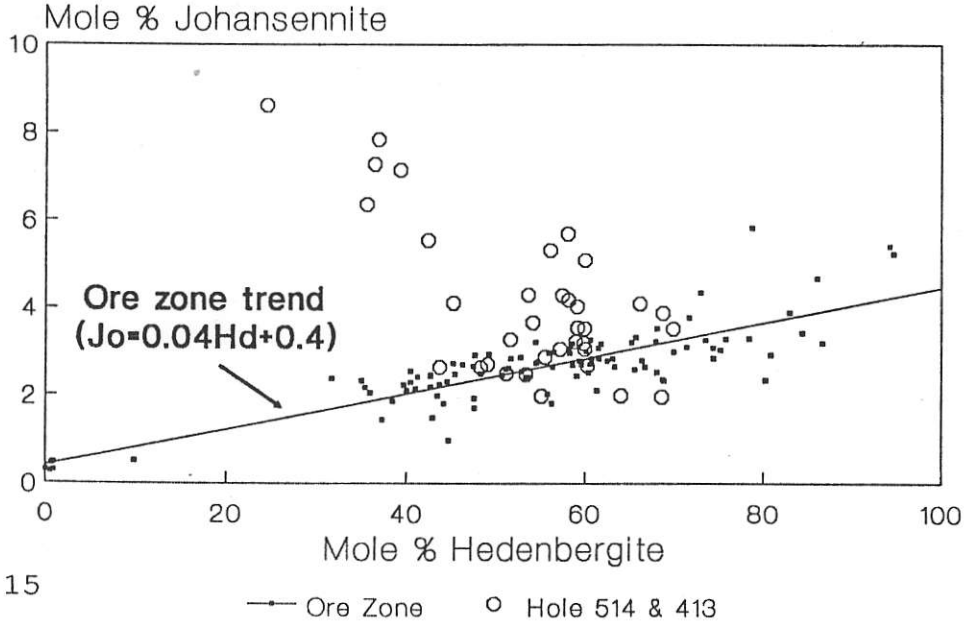

Figure 15

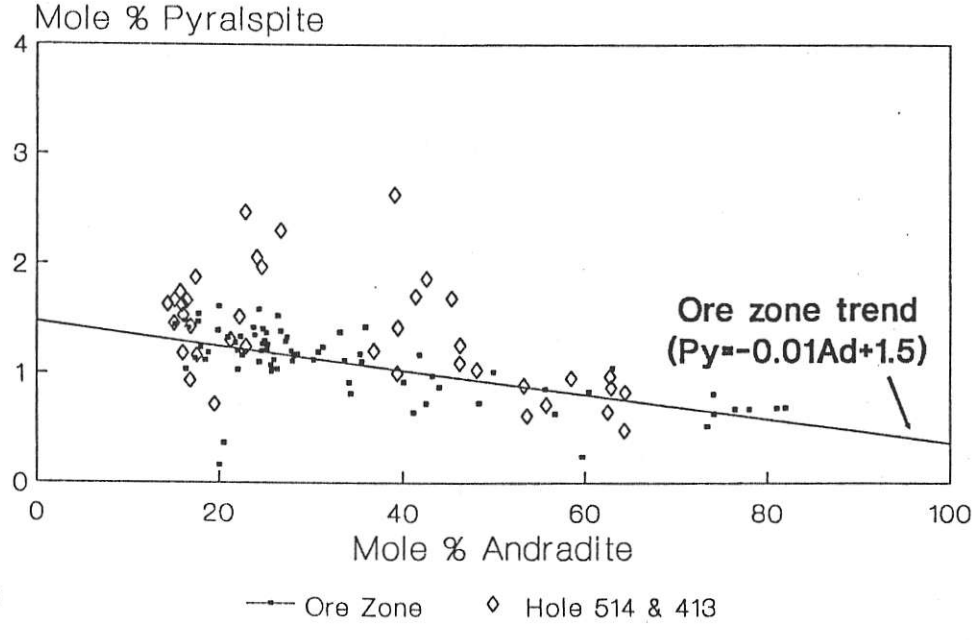

Figure 16

A.

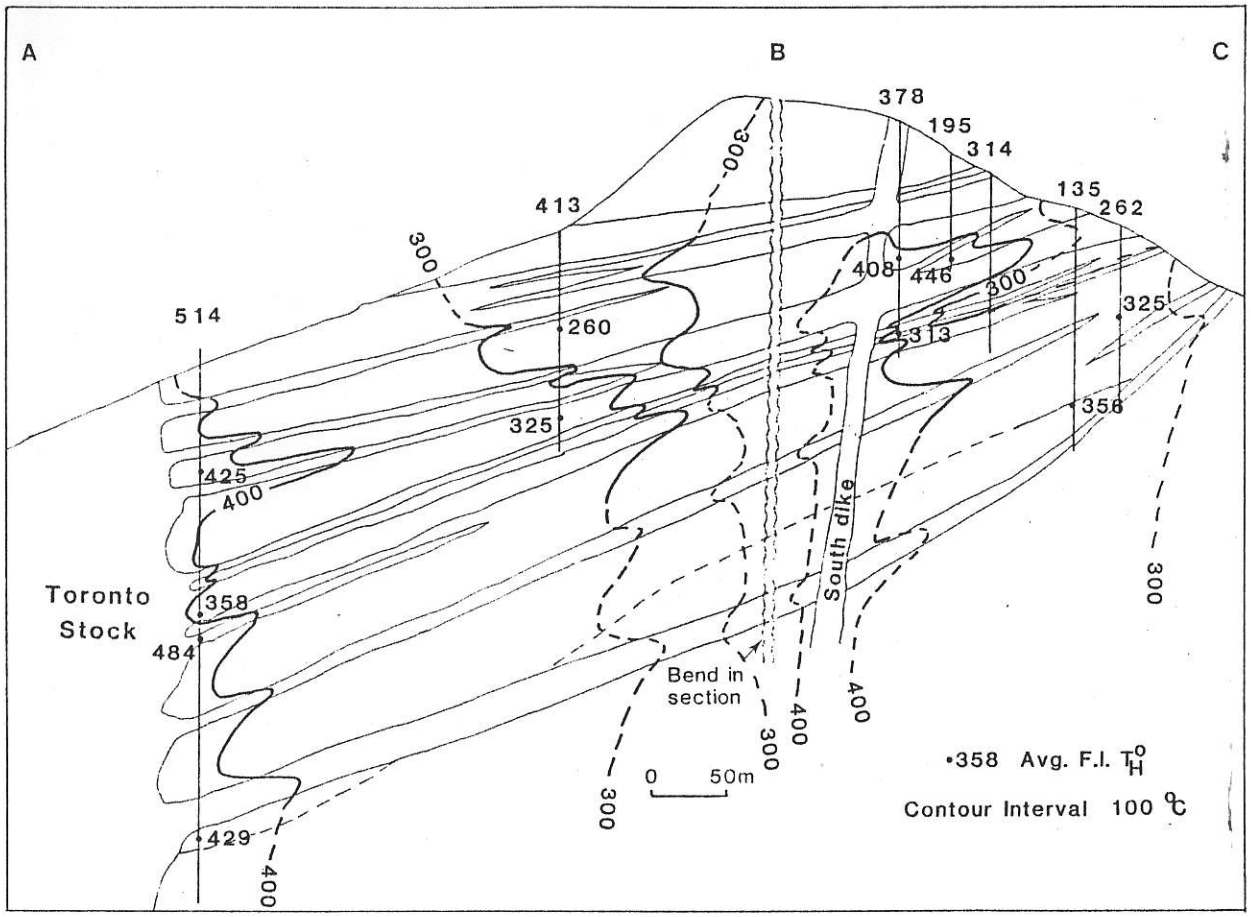
A
B
C
378
195
314
135
262
413
514
260
325
313
358
425
400
Toronto
Stock
358
484
429
South dike
Bend in
section
0 50m
•358 Avg. F.I. T°H
Contour Interval 100 °C

Figure 17

B.

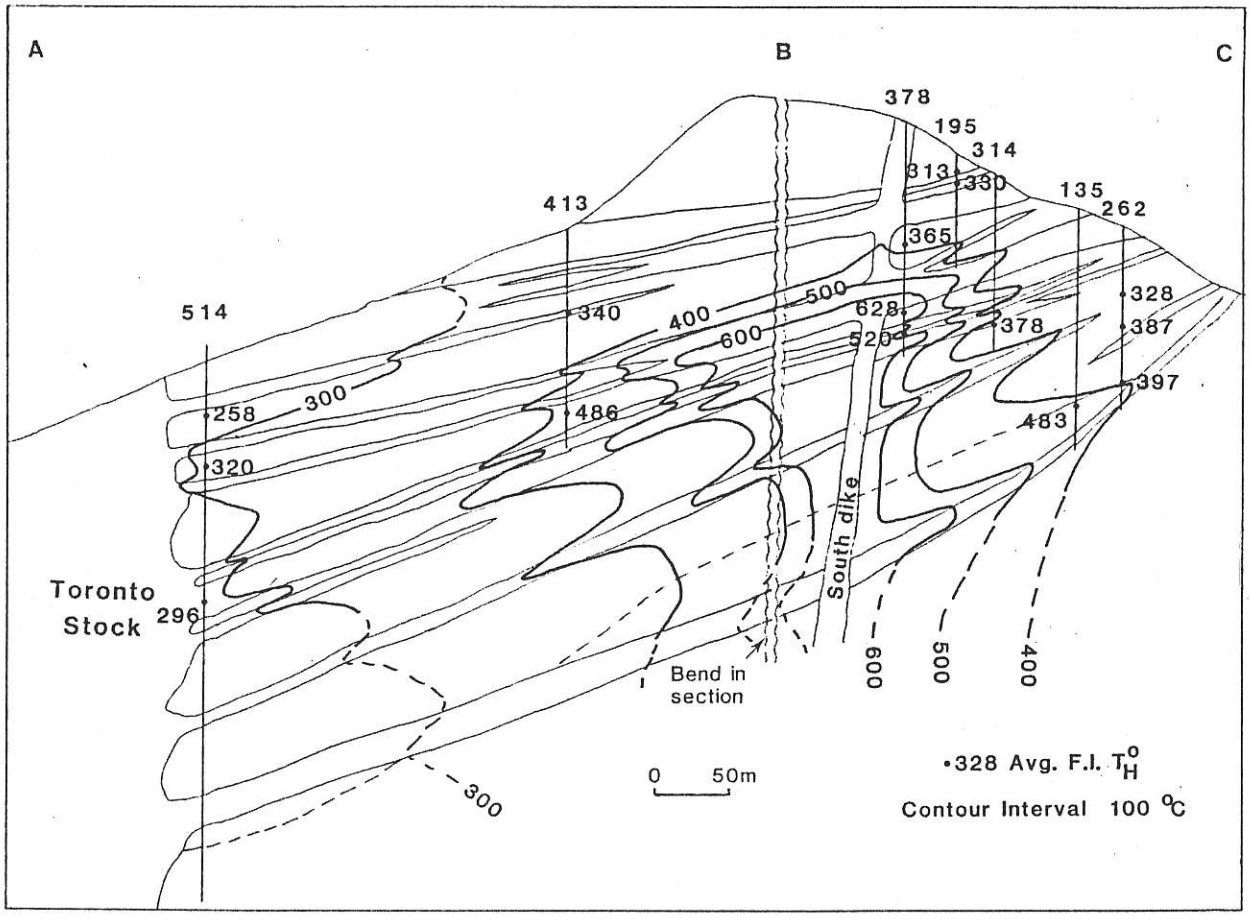
A
B
C
378
195
314
313
330
135
262
365
413
514
340
400
500
628
520
378
328
387
397
483
258
300
486
320
Toronto
Stock
296
South dike
Bend in
section
0 50m
•328 Avg. F.I. T°H
Contour Interval 100 °C

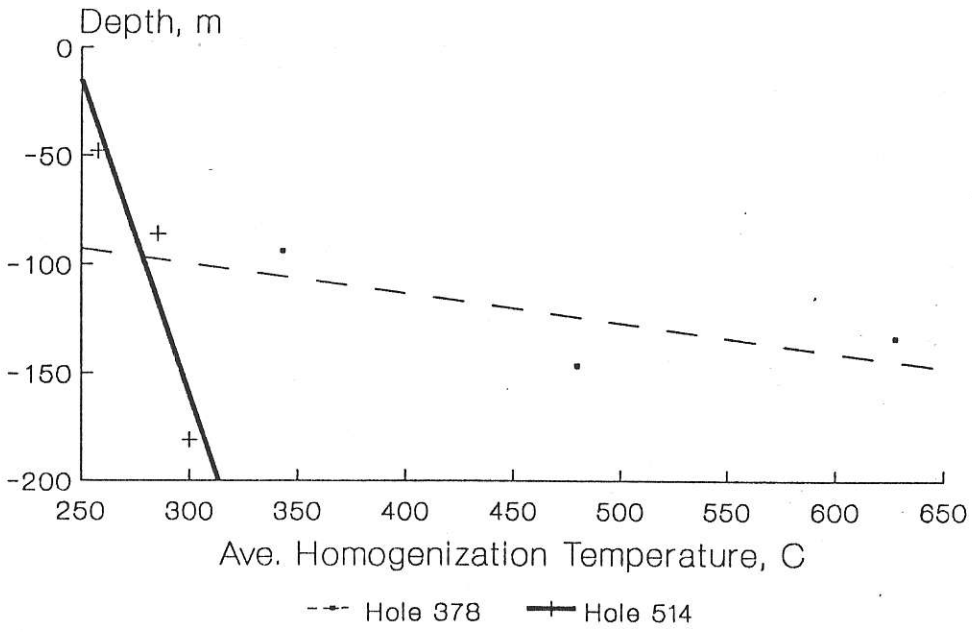

Figure 18

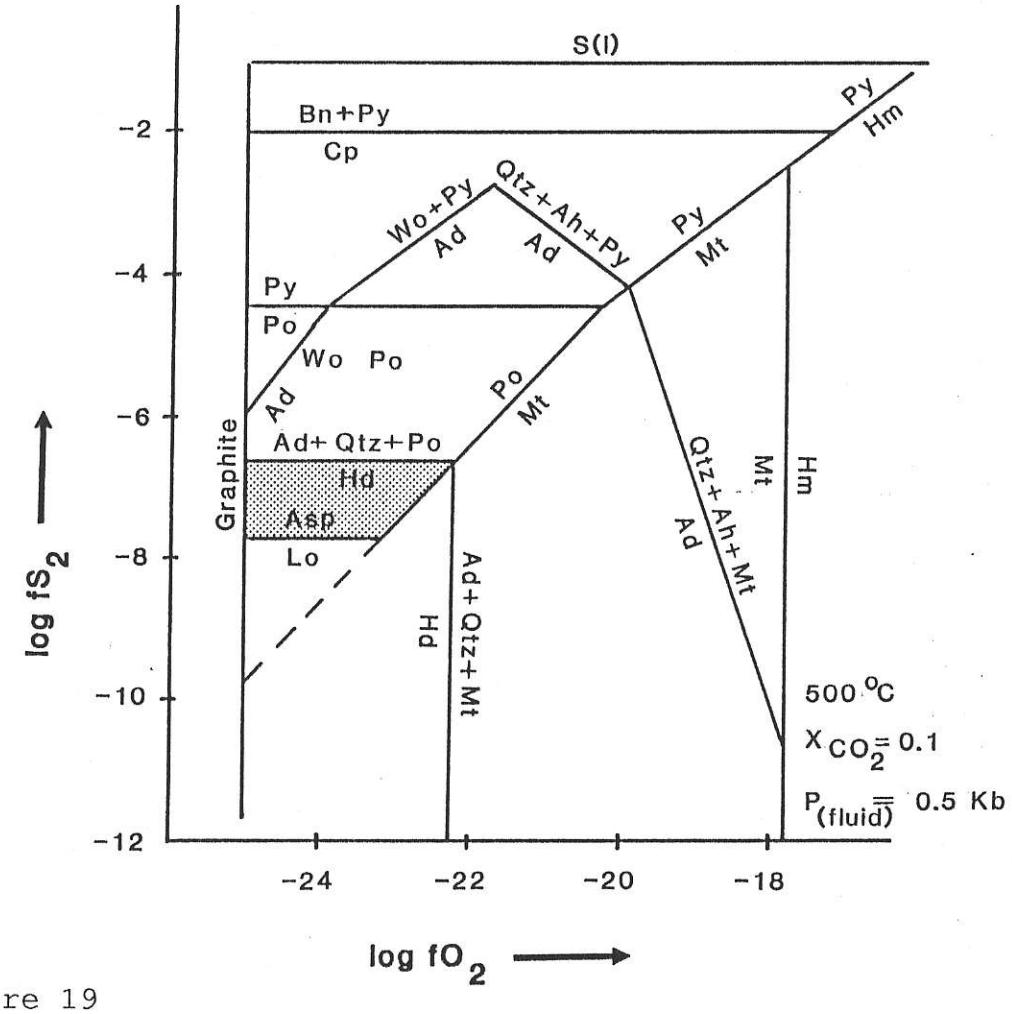

Figure 19

A.

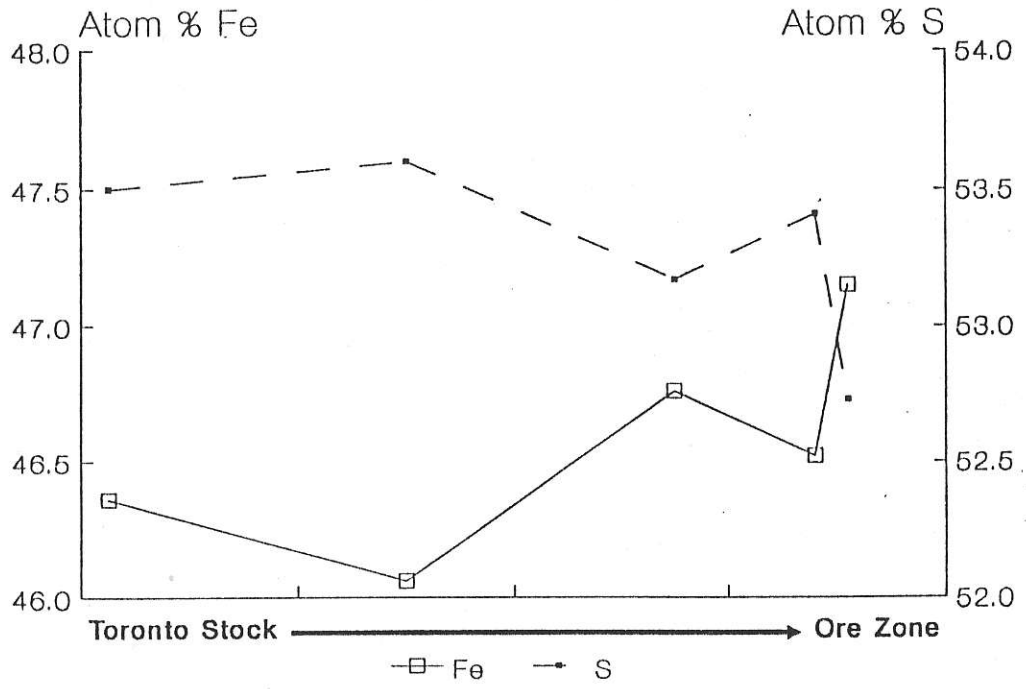
Atom % Fe
Atom % S
48.0
47.5
47.0
46.5
46.0
54.0
53.5
53.0
52.5
52.0
Toronto Stock
Ore Zone
Fe
S

B.

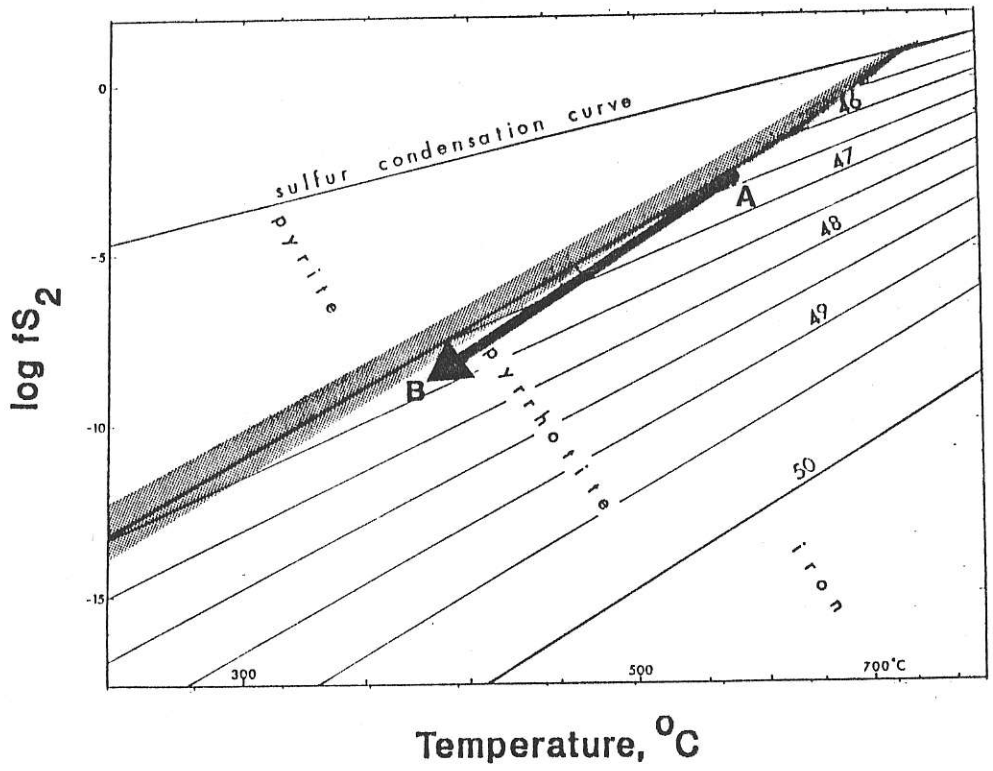
sulfur condensation curve
pyrite
pyrrhotite
iron
A
B
46
47
48
49
50
0
-5
-10
-15
300
500
700°C
log fS2
Temperature, °C

Figure 20

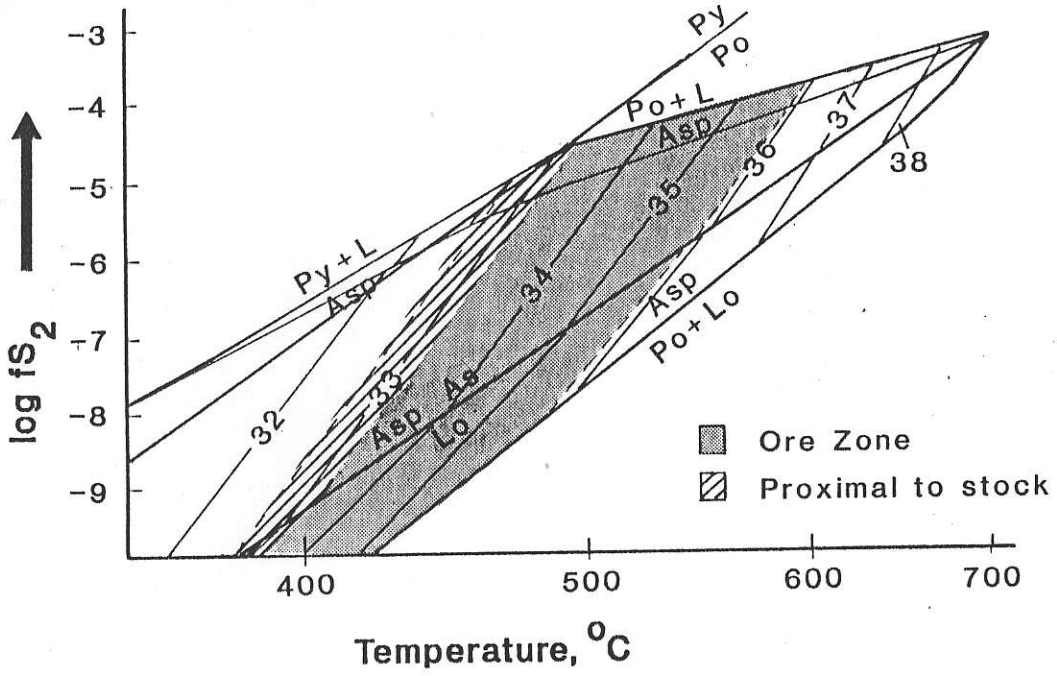

Figure 21

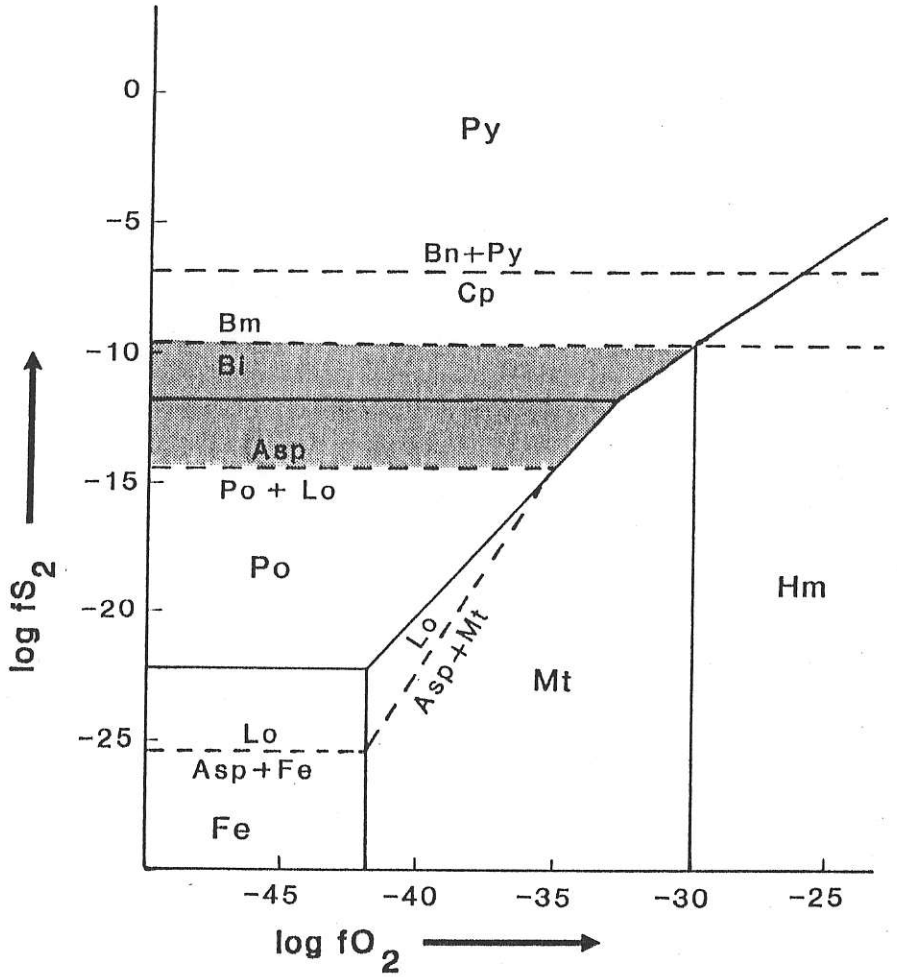

Figure 22

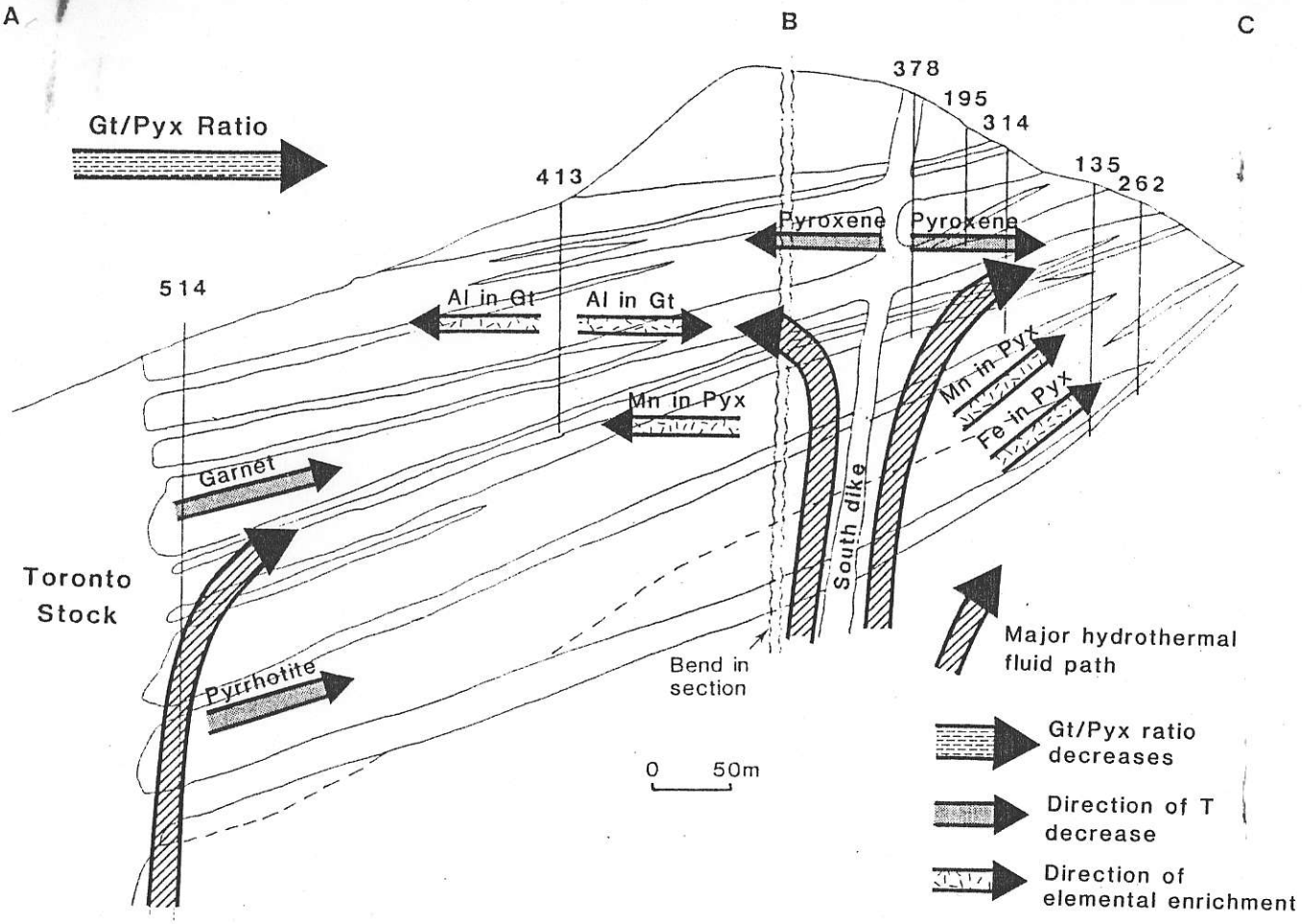
A
B
C
Gt/Pyx Ratio
514
413
378
195
314
135
262
Pyroxene
Pyroxene
Al in Gt
Al in Gt
Mn in Pyx
Mn in Pyx
Fe in Pyx
Garnet
Toronto
Stock
Pyrrhotite
South dike
Bend in
section
0 50m
Major hydrothermal
fluid path
Gt/Pyx ratio
decreases
Direction of T
decrease
Direction of
elemental enrichment

Figure 23